photonics

MDPI

Review

Advances in Multicore Fiber Grating Sensors

Zhiyong Zhao [1], Yunli Dang [1,*] and Ming Tang [1,2]

[1] Wuhan National Lab for Optoelectronics (WNLO), School of Optical and Electronic Information, Huazhong University of Science and Technology, Wuhan 430074, China; zhiyongzhao@hust.edu.cn (Z.Z.); tangming@mail.hust.edu.cn (M.T.)
[2] Optics Valley Laboratory, Wuhan 430074, China
* Correspondence: yunlidang@hust.edu.cn

Abstract: In recent years, multicore fiber (MCF) has attracted increasing interest for sensing applications, due to its unique fiber structure of multiple parallel cores in a single fiber cladding, which offers a flexible configurable platform to establish diverse functional fiber devices for sensing applications. So far, a variety of discrete fiber sensors using MCF have been developed, among which one of the major categories is the MCF grating sensors. The most distinct characteristic of MCF that differs from the normal single mode fibers is that the off-center cores of a MCF are sensitive to bending, which is caused by the bending induced tangential strain in off-center waveguides through either compression or stretching. The bending sensitivity has been widely developed for bending/curvature sensing or measuring physical parameters that are associated with bending. In this paper, we review the research progress on MCF-based fiber grating sensors. MCF-based diverse fiber grating sensors will be introduced, whose working principles will be discussed, and various types of applications of the MCF grating sensors will be summarized. Finally, the challenges and prospects of MCF grating for sensing applications will be presented.

Keywords: multicore fiber; fiber Bragg grating; long period grating; fiber grating sensors

check for updates

Citation: Zhao, Z.; Dang, Y.; Tang, M. Advances in Multicore Fiber Grating Sensors. *Photonics* **2022**, *9*, 381. https://doi.org/10.3390/photonics9060381

Received: 30 January 2022
Accepted: 9 March 2022
Published: 26 May 2022

Publisher's Note: MDPI stays neutral with regard to jurisdictional claims in published maps and institutional affiliations.

Copyright: © 2022 by the authors. Licensee MDPI, Basel, Switzerland. This article is an open access article distributed under the terms and conditions of the Creative Commons Attribution (CC BY) license (https://creativecommons.org/licenses/by/4.0/).

1. Introduction

In recent years, multicore fiber (MCF) technology has been extensively investigated for applications spanning optical fiber transmission, sensing and laser [1–6], etc. Thanks to the promotion of bandwidth requirement in the field of optical fiber communications, the MCF-based space-division multiplexing technique has developed rapidly in the last decade as a promising solution to increase the transmission capacity per fiber [7], which has substantially facilitated the development of MCF manufacturing and the relevant optical components. On the other hand, since multiple spatial cores of the MCF allow for independent parallel optical transmission within a single fiber, the unique MCF also turns out to be a flexible configurable platform that allows to develop diverse functional fiber devices and systems for sensing applications.

Multicore fiber contains more than one core in a single fiber cladding, whose core numbers and their spatial distributions can be flexibly designed in terms of the tolerance of inter-core crosstalk. Some common core arrangements of MCF include hexagonal structure [8], square lattice structure [9], ring structure [10], and linear array structure [11], etc. On the other hand, MCF can be manufactured with homogeneous or heterogeneous fiber cores, depending on the used material compositions of the cores, i.e., the cores of a homogeneous MCF have identical refractive index profiles, while those of the heterogeneous MCF are not the same. Currently, most of the MCFs are weakly-coupled MCFs, whose core-to-core pitch is deliberately set to be large (generally >30 um) in order to avoid high crosstalk between adjacent cores [12]. As a result, the weakly-coupled MCFs can transmit optical signals independently in different spatial cores. In addition, some effective fiber structure designs have been proposed to suppress inter-core crosstalk, including the

trench-assisted cladding structure and the air-hole-assisted cladding structure [2,13], etc. However, in contrast, strongly coupled MCFs have also been developed recently, whose cores are much closer to each other in comparison with the weakly coupled MCFs. This kind of MCF supports super-modes transmission [14], which is therefore also considered as a form of multimode fiber. In a MCF-based optical system, one of the most critical optical components is the multiplexer/de-multiplexer (fan-in/fan-out), which is used to achieve optical coupling between each core of the MCF and the single mode fibers (SMFs). The proposed schemes include free space lens coupling [15,16], waveguide coupling [17], and etched or tapered fiber bundle coupling [8,18–21], etc.

Multicore fiber possesses some outstanding advantages, including multiple independent spatial channels, all-solid cores, small size and compact, excellent mechanical robust properties, etc. Specifically, different from the situation in the normal SMFs, where the cores are located in the fiber center, i.e., the strain neutral axis, the off-center cores of MCF are sensitive to bending, since fiber bending will generate tangential strain in off-center positions of the waveguide. The bending sensitivity has been used to develop various bending/curvature sensors, as well as to measure some other physical parameters that are associated with bending, e.g., vibration, acceleration, flow velocity of liquid and gas, etc. MCF sensors can be divided into two categories, i.e., distributed fiber sensors and discrete fiber sensors [22,23]. On one hand, MCF-based distributed fiber sensors have shown unprecedented performance that allows for distributed curvature and 3-D shape sensing [24]. In addition, MCF space-division multiplexed system configurations also turn out to be effective solutions of many critical problems in conventional distributed sensors, e.g., addressing the intrinsic cross-sensitivity issue in Brillouin distributed sensors [25,26], enabling large dynamic range and ultra-high measurement resolution simultaneously [27], achieving multi-parameter sensing [28,29], as well as extending the sensing range and frequency measurement range [30,31], etc. On the other hand, so far, a variety of discrete fiber sensors using MCF have been developed, which can roughly be categorized into two types, including the MCF grating sensors and the MCF interferometric sensors. MCF gratings sensors are one of the major categories of MCF discrete sensors, where fiber gratings are written in the cores of MCF. In addition, the multi-core structure of the MCF provides an excellent platform to fabricate in-fiber spatially integrated interferometers by means of splicing with other fibers or tapering, as well as using the fan-in/out coupler [32–34], etc., as shown in Figures 1 and 2, respectively.

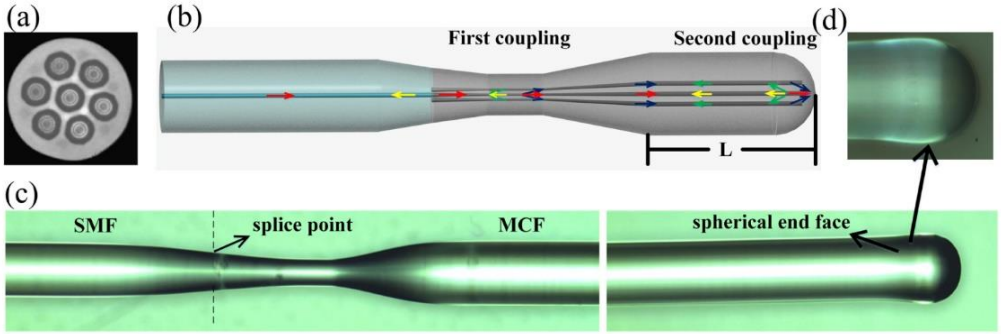

Figure 1. MCF sensor fabricated with tapering. (**a**) The cross-section image of the MCF. (**b**) Schematic diagram and operation principle of the Michelson-type multipath interferometer. (**c**) MCF-MI structure under microscope. (**d**) Spherical end face of MCF under microscope. Reprinted with permission from Ref. [34] © 2016 Optica Publishing Group.

In this paper, we review the research progress of fiber grating sensors that are using multicore fibers. Firstly, the unique bending sensitivity in off-center cores of MCF will be introduced in Section 2. Then, the advances in MCF-based fiber Bragg grating (FBG) sensors, tilted fiber Bragg grating (TFBG) sensors, and long-period grating (LPG) sensors will be summarized thoroughly, which will be presented in Section 3, Section 4, and Section 5,

respectively. Section 6 will discuss the challenges and future prospects of MCF grating sensors. Finally, a conclusion will be given in Section 7.

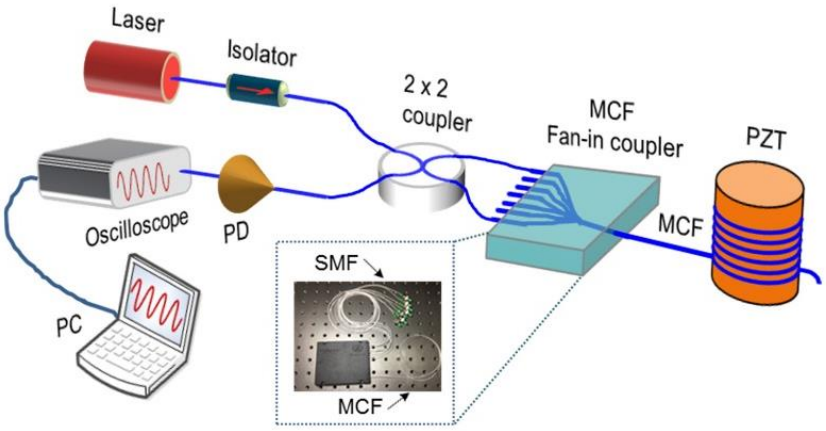

Figure 2. MCF Michelson interferometer sensor fabricated by using the fan-in/out coupler. Reprinted with permission from Ref. [33] © 2018 Optica Publishing Group.

2. Bending Sensitivity in Off-Center Cores of MCF

There has been increasing interest in developing various MCF grating sensors, including MCF-based FBG, TFBG, and LPG sensors, etc. It is well-known that SMF-based fiber grating sensors have been widely used for measuring temperature and strain, etc. The fiber core of SMF is located on the strain neutral axis, so theoretically FBG that is inscribed in the central core of a SMF is not sensitive to bending, as bending will not give rise to strain to the FBG. While in a bent MCF, as shown in Figure 3, the cores on the outer side of the neutral plane will be stretched, and the cores on the inner side of the neutral plane will be compressed, as a result fiber bending will give rise to tangential strain in off-center cores [24,31,35]. The fiber gratings written in the off-center cores of MCF will thus be sensitive to bending, due to fiber bending induced strain. By using the unique bending sensitivity, MCF has been widely used for bending sensing and relevant applications.

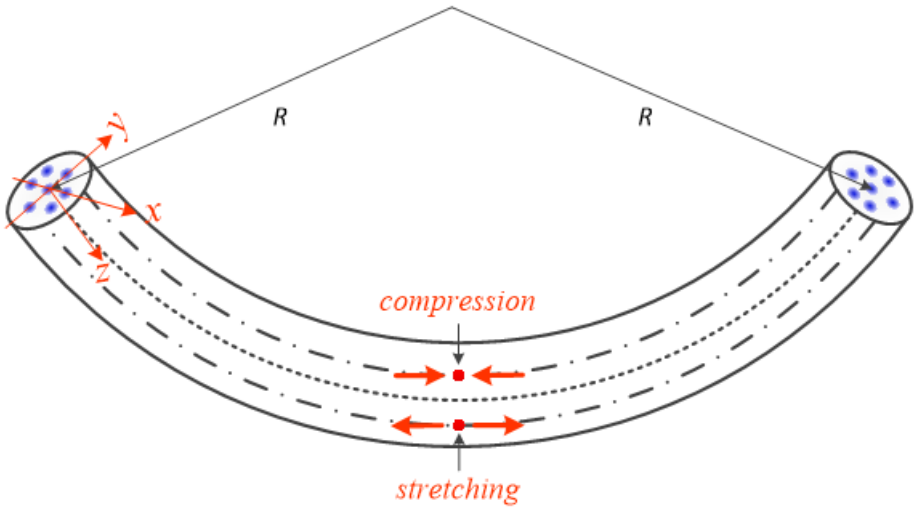

Figure 3. Schematic diagram of a bent MCF with a bending radius of R. The inner side cores will be compressed, while the outer side cores will be stretched. As a result, bending will generate different local tangential strains in distinct spatial cores. Adapted with permission from Ref. [31] © 2018 IEEE.

Let us take a seven-core fiber as an example, as shown in Figure 4 [36]. Fiber bending induced local tangential strain in MCF can be quantitatively determined, as given by [24,35]

$$\varepsilon_i = -\frac{d_i}{R}\cos(\theta_b - \theta_i) \tag{1}$$

where d_i is the distance of core i to the fiber center, R is the bending radius ($\kappa = 1/R$), θ_b is the bending angle which is defined to be the angular offset from the local x-axis to the local fiber bending direction, and θ_i is the angular position of core i, i.e., the angle from local x-axis to a specific core i. It is worth noticing that for the central core $d = 0$, so it can be inferred from Equation (1) that fiber bending will not generate strain in the central core of MCF.

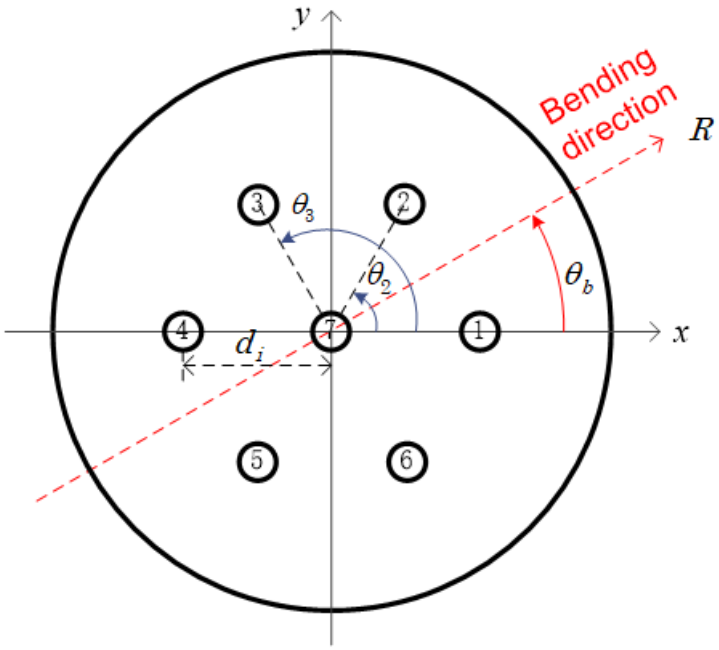

Figure 4. The transversal spatial distribution of cores of a seven-core fiber, showing the definitions of some important geometrical parameters. Reprinted with permission from Ref. [36] © 2016 Optica Publishing Group.

3. MCF-Based Fiber Bragg Grating Sensors

The first demonstration of bending sensing using fiber Bragg gratings in MCF was reported by Gander et al. [37]. Since fiber bending will give rise to local tangential strain in off-center cores, assuming that two cores are in the bending plane, then the strain difference between the two cores is determined by

$$\Delta\varepsilon = \varepsilon_1 - \varepsilon_2 = \frac{2d}{R} \tag{2}$$

Note that this fiber bending induced tangential strain in off-center cores will lead to the shift of Bragg wavelengths of FBGs, as a result the difference in Bragg wavelength between two adjacent gratings written in different cores can be used to retrieve the local curvature, as governed by

$$\Delta\lambda_B = \lambda_B(1 - p_\varepsilon)\Delta\varepsilon \tag{3}$$

where p_ε is the effective photo-elastic coefficient. Equation (3) indicates that the Bragg wavelengths difference is proportional to the strain difference $\Delta\varepsilon$, and thus the curvature. Therefore, curvature can be obtained from the measurement of two FBGs. The benefit of the MCF-based curvature sensor is that it is temperature-independent, because the two FBGs in the MCF have almost identical temperature sensitivities.

By using a pair of FBGs in two cores of the MCF, it is only able to measure a one-axis bending, while in order to measure a two-axis bending, two pairs of orthogonal FBGs in three cores are required [38], e.g., cores 1–3 in Figure 5a, where the difference between the wavelength shifts in each grating pair reveals the differential strain and hence the curvature. For a specific azimuthal placement of the four-core fiber, bending sensitivity of the FBGs has been calibrated by bending the fiber in the horizontal and vertical (i.e., x and y) planes separately. The Bragg wavelength differences between the two core pairs (i.e., cores 1 and 2, cores 2 and 3) are plotted in Figure 5b,c, respectively [38].

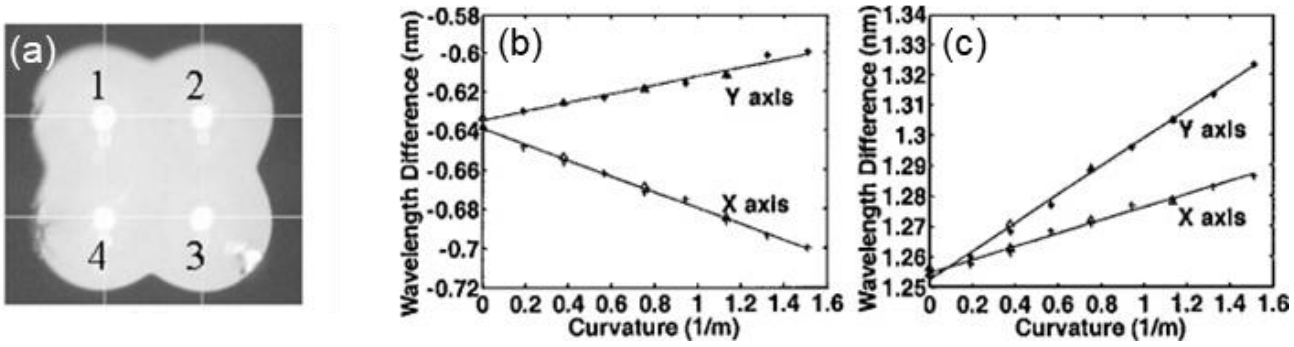

Figure 5. (**a**) The cleaved face of the four-core fiber. (**b**,**c**) are the measured wavelength difference versus applied curvature for x-axis and y-axis bending with a linear least-square fit: (**b**) pairing of cores 1 and 2; (**c**) pairing of cores 2 and 3. Adapted with permission from Ref. [38] © 2003 Optica Publishing Group.

Note that by using the two pairs of FBGs, their wavelength difference can be described by a matrix in terms of curvature κ_x and κ_y, as given by

$$\begin{bmatrix} \Delta\lambda_{12} \\ \Delta\lambda_{23} \end{bmatrix} = \begin{bmatrix} \Delta\lambda_{12}^0 \\ \Delta\lambda_{23}^0 \end{bmatrix} + \begin{bmatrix} p & q \\ r & s \end{bmatrix} \begin{bmatrix} \kappa_x \\ \kappa_y \end{bmatrix} \tag{4}$$

where $\Delta\lambda_{12}^0$ and $\Delta\lambda_{23}^0$ are the constant absolute wavelength difference between FBGs, p, q, r, and s are the calibrated response coefficients of FBGs along the two bending axes. Inverse matrix transformation can then be performed to determine the relative bending in the x and y axes, so two-axis curvature measurement is achieved.

The result indicates that the responses of FBGs under different bending angle are distinct. As a matter of fact, it can be inferred from Equation (1) that the curvature sensitivity (wavelength shift vs. curvature variation) of an outer core should be angular position dependent, which is subject to a cosinoidal function with respect to the angular offset between the fiber core and the bending direction, i.e., $\theta_b - \theta_i$. The offset angle dependence of the curvature sensitivity of the off-center core has been investigated, whose experimental setup is shown in Figure 6a [39]. The setup allows to adjust the curvature of the sensing fiber, as well as to rotate the fiber with about 2° angular accuracy. Here, the curvature κ of the sensing fiber is governed by [39,40]

$$\sin\left(\frac{L\kappa}{2}\right) = \frac{(L - \Delta L)\kappa}{2} \tag{5}$$

where L is the initial length between the two fixed ends of the fiber without bending and ΔL is the movement distance of the adjustable stage.

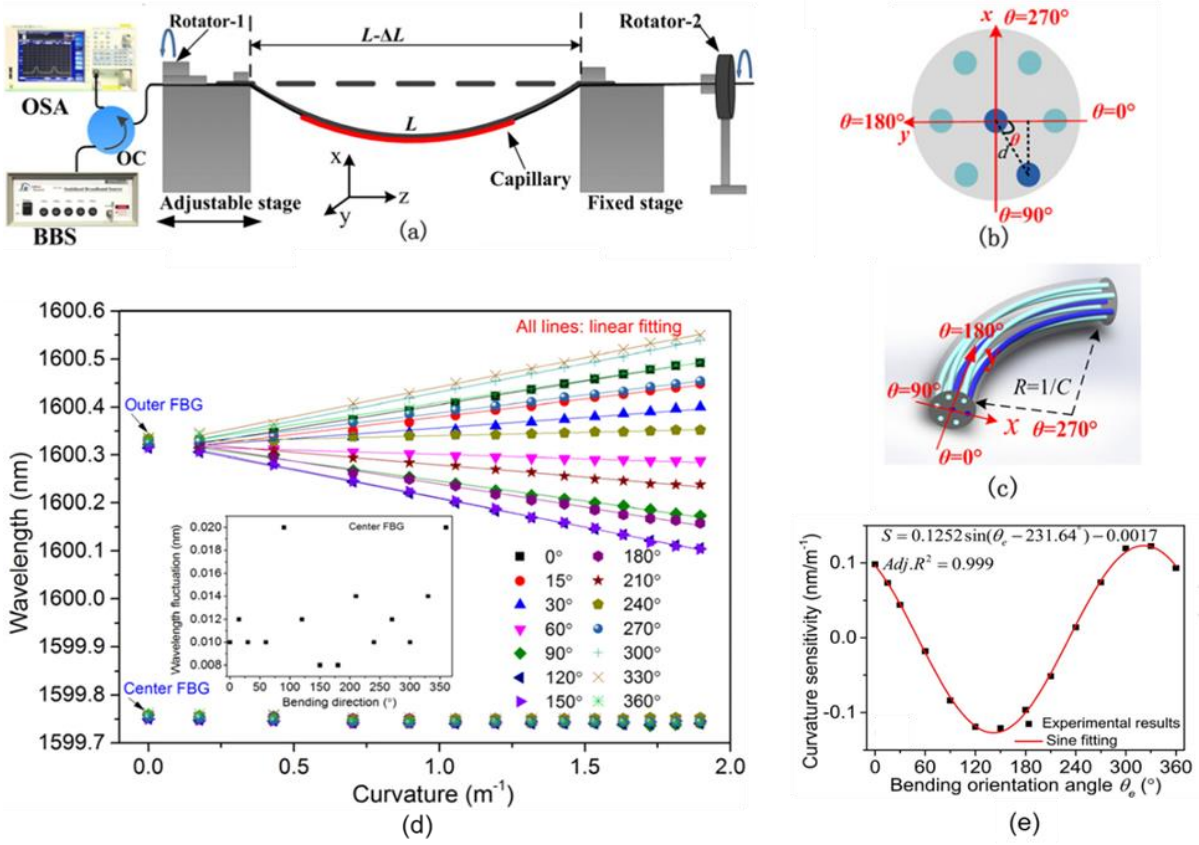

Figure 6. (**a**) Experimental setup of the proposed curvature sensor; (**b**) theoretical definition of the bending orientation angle; (**c**) schematic diagram of a curved fiber when the bending angle is 270°; (**d**) Bragg wavelength shifts versus curvature for the two FBGs at different bending angles. The inset shows the wavelength fluctuations of the central FBG at different bending angles over the curvature range from 0 to 1.896 m^{-1}. (**e**) Relationship between the curvature sensitivity of FBG in the off-center core and the experimental bending orientation angle. Adapted with permission from Ref. [39].

As shown in Figure 6b, a heterogeneous seven-core fiber was used in the experiment, while only one outer core and the central core have been used for characterization. A schematic diagram of the curved fiber with 270° bending angle is presented in Figure 6c. By rotating the fiber, a different bending angle (i.e., the angular offset) with respect to the selected fiber core can be generated, note that the initial state is trivially considered to be 0°; meanwhile for each applied bending angle, the Bragg wavelength shifts under different curvatures were measured, and the result is plotted in Figure 6d. It is observed that for each specific bending angle, the Bragg wavelength shift of FBG in the outer core is linear to the curvature of the sensing fiber, and different bending angle leads to distinct curvature sensitivities. In contrast, as shown in Figure 6d, the Bragg wavelengths of FBG in the central core remain almost unchanged under different curvature, so it turns out that it is not sensitive to bending, because the FBG is located on the strain neutral axis of the fiber. Using the measurement results of Figure 6d, the obtained curvature sensitivities of FBG in the off-center core as a function of the bending angles is presented in Figure 6e. It verifies that the curvature sensitivity of FBG in the off-center core varies with the relative bending angle. Specifically, as indicated by Equation (1), it follows a cosinoidal (or sinusoidal) function with respect to the bending angle, and a period of 360°. Since the FBG in the central core is insensitive to fiber bending, it can be used to compensate the effects of temperature and externally applied axial strain.

The bending angle dependence of the curvature sensitivity of a specific off-center core has been investigated in a twin-core few-mode fiber (TC-FMF) [41]. As shown in Figure 7, each core of the TC-FMF supports LP_{01} and LP_{11} modes. While three resonance peaks

were observed in the FBG reflection spectrum of the TC-FMF, which result from the LP_{01} mode resonance, LP_{01}–LP_{11} mode cross-coupling resonance, and LP_{11} mode resonance, respectively. The bending response of one resonance peak has been investigated by rotating the fiber from 0° to 360° with a step of 15°, and the measurement was then repeated for some different curvatures of the sensing fiber. The result is shown in Figure 8a. It indicates that for a specific fiber curvature, the resonance wavelength varies periodically with respect to the bending angle, which matches well with the inference of Equation (1). The curvature sensitivities (wavelength shift vs. curvature variation) can then be calculated from the measurement result, which is shown in polar coordinate in Figure 8b. The result indicates that the curvature sensitivity reaches to the maximum when the bending angle is 0° (or 360°) and 180°, which is because the used sensing fiber core is located in the bending plane and bending caused strain is the maximum in this case, as inferred from Equation (1); while the curvature sensitivity is zero when the bending angle is 90° and 270°, which is because the used sensing fiber core is located in the strain neutral axis plane in this case, as a result bending will not give rise to strain in the fiber core.

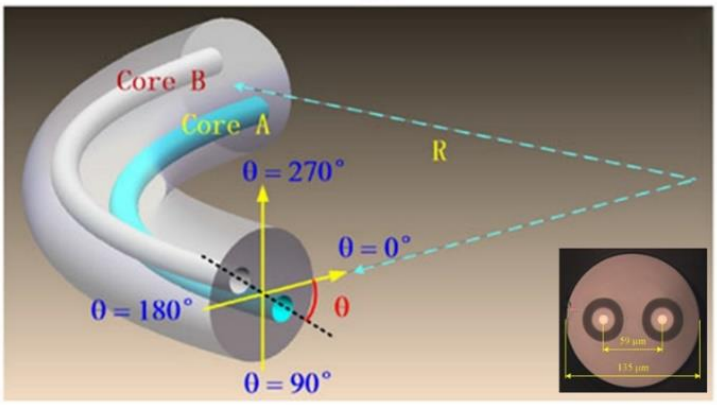

Figure 7. Schematic diagram of a curved twin-core few-mode fiber with bending radius of R, where bend direction angle θ is the angular offset between the fiber bend plane and the axis connecting core A and core B. The inset shows the microscopic image of the TC-FMF. Adapted with permission from Ref. [41] © 2017 IEEE.

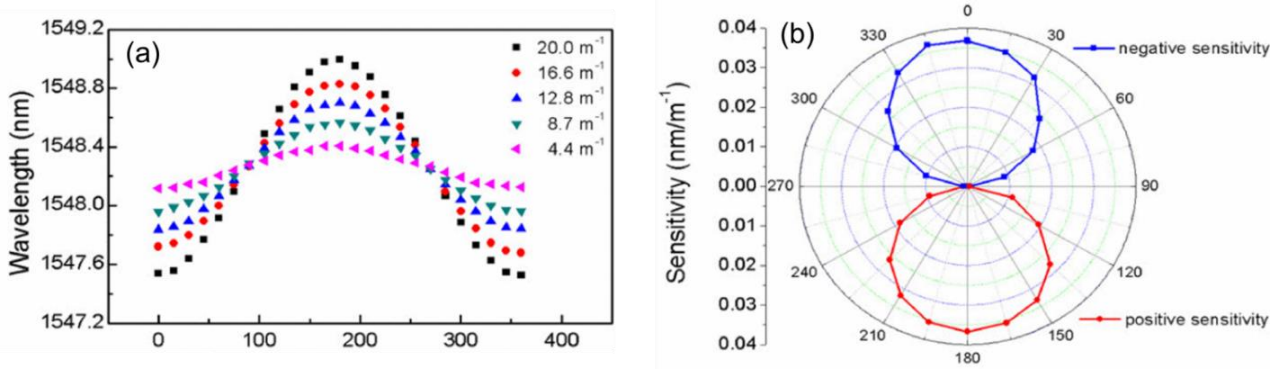

Figure 8. (**a**) Resonant wavelength of one peak in the reflection spectrum of TC-FM FBG as a function of the bend direction angle under different bend curvatures. (**b**) Bend sensitivities of the TC-FM FBG in different bend directions. Adapted with permission from Ref. [41] © 2017 IEEE.

The bending responses of all the three resonance peaks have also been compared. For a given bending direction, different bending radii were applied to the sensing fiber, meanwhile the reflection spectra were recorded, respectively, as shown in Figure 9a. The wavelength shifts of the three peaks as a function of the curvature are shown in Figure 9b. The linearly fitted curvature sensitivities are −36.26, −37.41, and −36.35 pm/m^{-1}, respectively. Therefore, it turns out that there is no large difference between the resonance peaks in terms of the response of fiber bending.

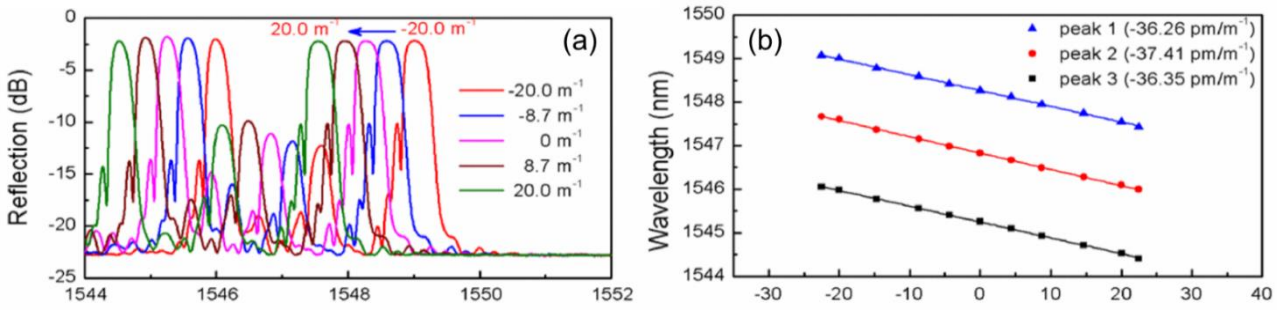

Figure 9. Bend response of the TC-FM FBG with different bend curvatures. (**a**) Reflection spectra evolution of the TC-FM FBG with different bend curvatures. (**b**) Wavelength shift of the three resonance peaks in the reflection spectra of the TC-FM FBG as a function of bend curvature. Adapted with permission from Ref. [41] © 2017 IEEE.

The curvature sensitivities of FBGs in all the off-center cores of a seven-core fiber have also been characterized [42], as shown in Figure 10. For a given curved MCF with bending angle θ_b, as each outer core has different angular position θ_i, i.e., their relative angle offsets to the bending direction are distinct, the outer cores have different curvature sensitivities. While because the six outer cores are arranged hexagonally, the curvature sensitivities are actually the same with 60° offset in the polar coordinate between two adjacent outer cores.

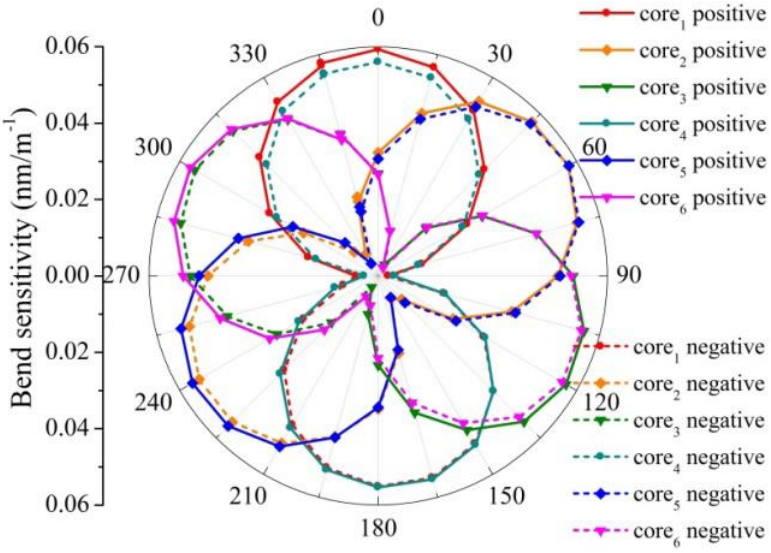

Figure 10. Bend sensitivities for the six outer-core FBGs in the seven-core fiber plotted for various bend directions (from 0° to 360°). Reprinted with permission from Ref. [42] © 2018 Optica Publishing Group.

In addition to the silica fiber, polymer optical fiber (POF) has also been investigated for bending sensing [43]. As shown in Figure 11a, the POF has off-center cores, in which Bragg grating is inscribed. Using the experiment setup shown in Figure 11b, bending was then applied to the sensing fiber along four directions, i.e., 0°, 90°, 180°, and 270°, and the measured wavelength shifts as a function of the curvature is shown in Figure 11c. The fiber core is compressed along the 0° bending direction, and it is stretched along the 180° bending direction. While fiber bending should not give rise to strain in the fiber core along 90° and 270° bending directions, since the fiber core is in the neutral plane, and the wavelength shift of FBG along these two bending directions is assumed to be caused by misalignment of the fiber axis or a slight twist of the POF during measurement. The benefit of polymer fiber is that it has a smaller Young's modulus and its failure critical strain is much larger in comparison with the silica fiber, so it has potential in the bending sensing applications that have very small bending radius.

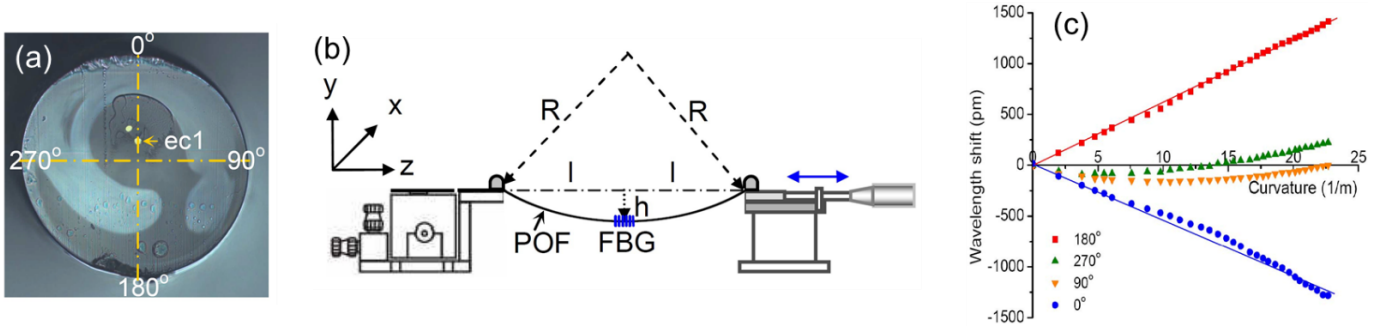

Figure 11. (**a**) Microscope image of the polymer fiber cross-section marked with the orientations; (**b**) schematic of the experimental setup for characterizing the FBG-based sensor. R is the bend radius and h is the displacement; (**c**) wavelength shifts of the eccentric polymeric FBG against curvatures at four different orientations. The symbols show the experimental data and lines depict the best-fit lines. Adapted with permission from Ref. [43] © 2010 IEEE.

It is realized that the most prominent advantage of FBG in MCF is that it allows for bending measurement, which is a unique characteristic that the FBG does not possess in the core of a normal SMF. As a matter of fact, FBG in MCF has also enabled the measurement of parameters that are associated with bending, e.g., transverse loading, acceleration, vibration, flow velocity of liquid and gas, etc.

For example, it is observed that when transverse loading is applied to an MCF, the reflection spectrum of FBG in the MCF will split due to transverse stress induced birefringence [44], as shown in Figure 12a, and it turns out that the splitting is a function of the applied loading, as shown in Figure 12b. It can be observed that the peak splitting of FBG is also angular position dependent for a given loading, because transverse stress is the largest around the cladding edge along the diameter that is aligned with the loading axis i.e., cores 1 and 3 in Figure 12b, and it is the lowest in the cores that are far from the loading axis, i.e., cores 2 and 4 in Figure 12b.

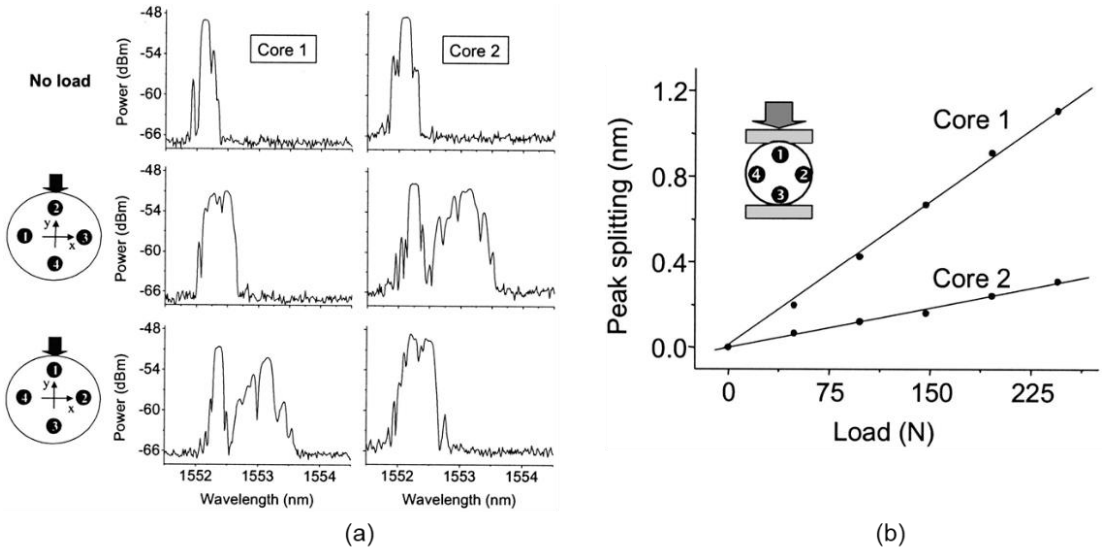

Figure 12. Birefringence-induced peak splitting due to increasing loading. Adapted with permission from Ref. [44] © 2004 Optica Publishing Group.

In fact, the orientation of transverse loading can also be retrieved from the measurement of FBG peak splitting in MCF. Because transverse loading induced birefringence is different at different angular positions, as a result the peak splitting of FBGs in different fiber cores is distinct as well, as is shown in Figure 12b. Therefore, the load angle relative to the cores can be found from the ratio of the Bragg peak splitting between pairs of cores [45].

This has been demonstrated by using FBGs that were inscribed at the same axial position in all cores of a four-core fiber, whose cores are arranged at the vertices of a square. Specifically, a parameter α that defines the ratio of peaking splitting coefficients (i.e., the slope of peaking splitting versus loading at a specific angle) of two adjacent cores is used to deduce the orientation of loading, as given by

$$\alpha = \frac{d\Delta\lambda_i}{dF} / \frac{d\Delta\lambda_j}{dF} \tag{6}$$

where $\Delta\lambda_i$ and $\Delta\lambda_j$ are the peak splitting of FBGs in two neighboring cores, F is the applied loading. The dependence of splitting coefficients ratio on loading angle is presented in Figure 13, where both the theoretical curve and experimental data are shown, and measurement was carried out by using two cores with 90° separation, i.e., cores 1 and 2 in the inset of Figure 13.

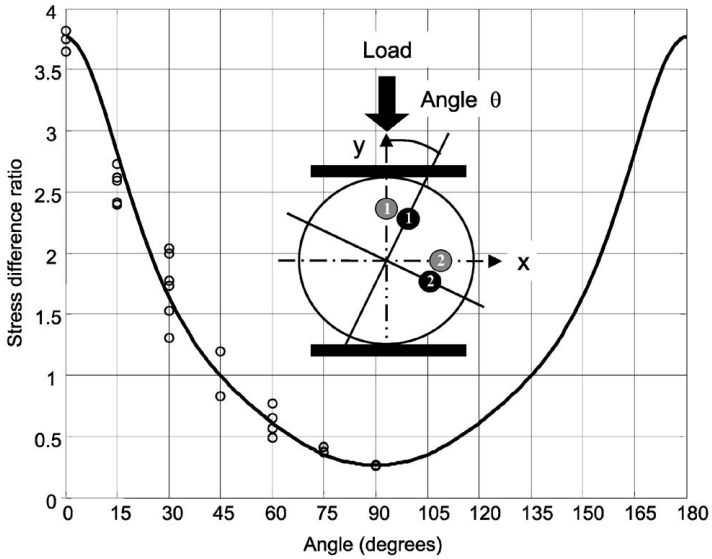

Figure 13. Theoretical curve (solid curve) and experimental data (points) for the stress difference ratio of two cores at 90° separation. Reprinted with permission from Ref. [45] © 2005 Optica Publishing Group.

Making use of the fiber bending induced differential strain between the FBGs in a four-core fiber, pitch and roll sensing has also been demonstrated [46]. As shown in Figure 14a, the four-core fiber was supported at one end and a small mass was attached to the other end of the fiber, so a cantilever is formed. The free end of the fiber trends to be curved due to gravity, thus, in this case the fiber bending induced differential strains between opposite grating pairs are determined by the orientation of fiber in pitch (in the vertical plane) and roll (azimuth) with respect to gravity. Specifically, the roll angle can be acquired from the ratio of the strain differences between two orthogonal core pairs, e.g., core pairs (1, 2) and (2, 3), as shown in the inset of Figure 14a. Moreover, the pitch angle can be achieved from the magnitude of the differential strain between pairs [46]. The measurement result of pitch and roll is shown in Figure 14b.

FBGs in a four-core fiber have also been used for dynamic two-axis curvature measurements by making use of the bending induced differential strain in off-center cores of the MCF [47]. For this application, in order to achieve dynamical strain measurement, arrayed waveguide grating (AWG) was used to interrogate the Bragg wavelength of the FBG by monitoring the optical power of different AWG channels, and then the ratio of the power in these channels was used to infer the grating wavelength, which permits strain measurement dynamically at kilohertz frequency.

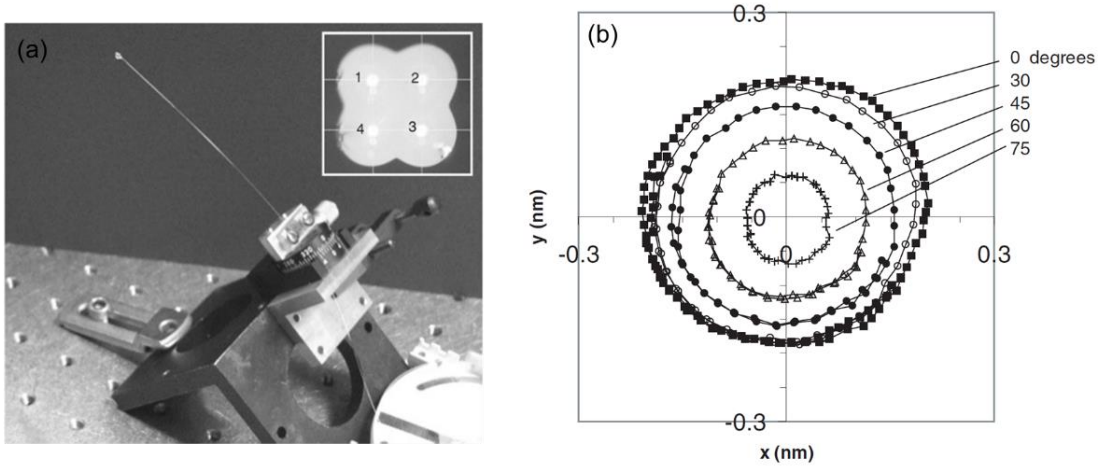

Figure 14. (**a**) Sensing fiber mounted in rotary stage; in this case the pitch angle is set at 45°. The inset shows the used four-core fiber in this experiment; (**b**) experimental results from pitch (θ) and roll (φ) measurements. $x = \lambda 1 - \lambda 2$, y = $\lambda 2 - \lambda 3$ are the differential Bragg wavelength shifts (in nm with offset removed) between orthogonal pairs (1, 2) and (2, 3) of MCF gratings. Data are plotted for θ = 0°, 30°, 45° (φ range 0–540°) and θ = 60°, 75° (φ range 0–360°). Adapted with permission from Ref. [46].

Note that the strain difference between two gratings in the MCF can be used to determine the radius of curvature R in the plane of the cores, as governed by

$$R = \frac{d}{\varepsilon_1 - \varepsilon_2} \tag{7}$$

where d is the distance between the cores and ε_n is the strain in the nth core. Therefore, the curvature in two dimensions can be obtained by using two orthogonal FBG pairs. As shown in Figure 15a, FBGs were written co-located in the cores of the MCF, and three cores have been used in the experiment. The MCF containing the FBGs was inserted into a stainless steel tube, and a cantilever was formed by clamping the tube at one end. A high speed camera was used to capture the displacement of the end of the cantilever during cantilever vibration at 28 Hz frequency; so that it can be used to compare with the result that was measured by the FBGs. Figure 15b presents the measured deflections by both the FBGs in MCF and the camera along x-axis and y-axis directions, showing good reliability.

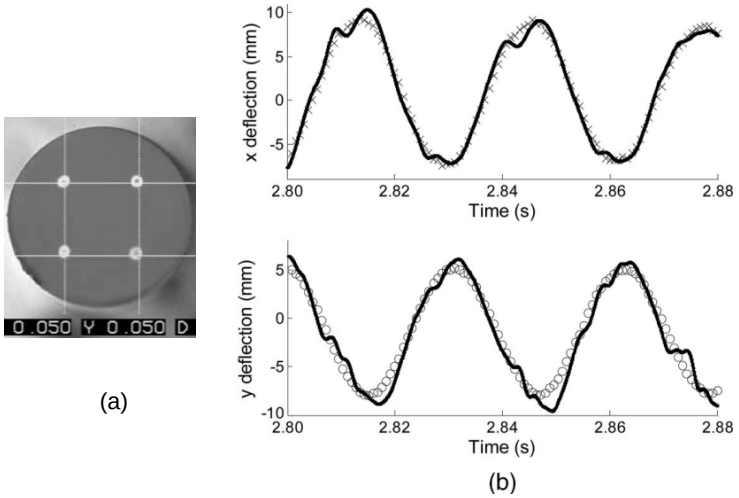

Figure 15. (**a**) Cross-section of the MCF. (**b**) Upper plot, x-deflection measured by MCF FBGs (solid curve) and camera (x). Lower plot, y-deflection measured by sensor (solid curve) and camera (o). Adapted with permission from Ref. [47] © 2006 Optica Publishing Group.

Based on the measurement of differential strain using FBGs in a four-core fiber, displacement sensing of the tunnel has also been demonstrated [48]. As shown in Figure 16, in order to measure displacement of the tunnel, the orientation calibrated MCF was mounted on two tunnel sections, as shown in Figure 16b, where FBGs are inscribed co-located in the cores of MCF. Figure 16c shows the schematic diagram of the displacement sensor. As explained previously, measurements of two orthogonal FBG pairs can be used to determine the two-axis curvature, and then the bending plane as well. For small deflection, once the curvature at a known position along the fiber cantilever is obtained, it can be used to determine the translational displacement δ, as governed by [48]

$$w''(x) = 12\frac{\delta}{L^2}\left(\frac{1}{2} - \frac{x}{L}\right) \tag{8}$$

where $w(x)$ is the displacement of the cantilever at a point x along the cantilever of length L, and $w''(x)$ is the second derivative of w.

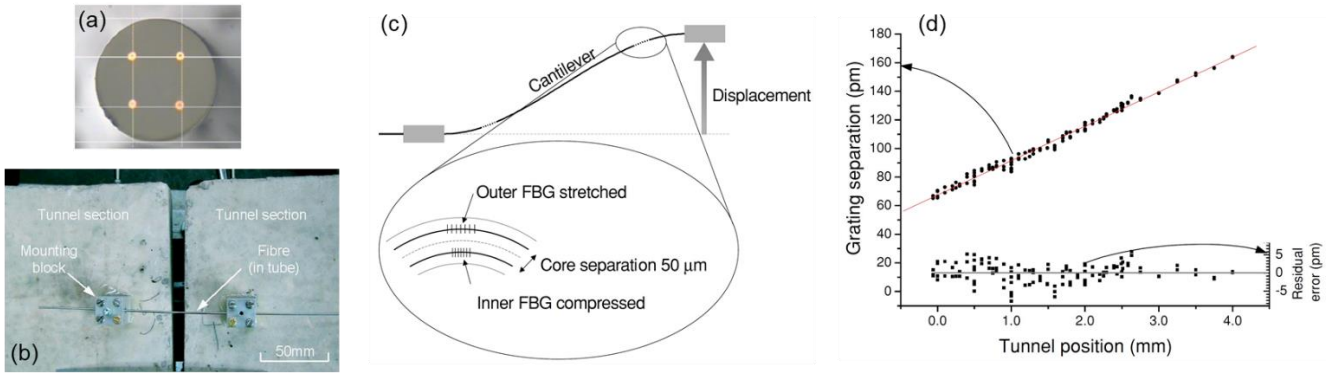

Figure 16. (**a**) Cross-section of MCF used in this experiment; (**b**) cantilever containing MCF attached to tunnel lining; (**c**) FBG pairs act as curvature sensors—the curvature is determined from the strain difference between the gratings; (**d**) experimental results from translation tests. Adapted with permission from Ref. [48].

The measurement of differential response between FBGs in a four-core fiber has also been developed for acceleration sensing [49]. The accelerometer consists of a short fiber cantilever with FBGs inscribed in the fiber cores near the clamping point, as shown in Figure 17a, where the inset shows the used four-core fiber. An epoxy mass is attached to the fiber end of the cantilever, as shown in Figure 17b, which helps to increases the sensitivity of the sensor.

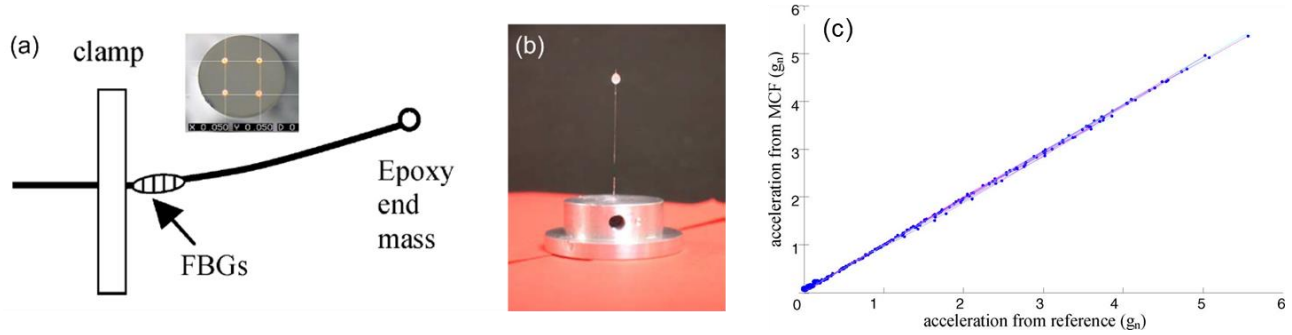

Figure 17. (**a**) Schematic diagram of the MCF cantilever-based accelerometer, the inset shows the four-core fiber used in the experiment; (**b**) the packaged acceleration sensor; (**c**) acceleration response of MCF accelerometer between 30 and 200 Hz. Adapted with permission from Ref. [49].

Using the same principle that has been explained previously, the measured differential strain between two adjacent FBG is used to determine the curvature ($1/R$) in the plane of the two cores, and by using two orthogonal pairs of cores, two-axis curvature measurement can be achieved. Then, acceleration a can be calculated once curvature is determined, as governed by [49]

$$a = \frac{EI}{m(x-l)} \cdot \frac{1}{R} \tag{9}$$

where E is the Young's modulus, I is the second moment of area of the fiber, m is the end mass, x is the distance of the measurement position from the clamp, and l is the length of the fiber cantilever. The measurement result of acceleration is shown in Figure 17c. On the other hand, it is worth mentioning that the frequency response of the sensor is also related to the cantilever length l and the fiber mass M, as given by [49,50]

$$f \propto \sqrt{\frac{3EI}{Ml^3}} \tag{10}$$

Therefore, the frequency response of the MCF-based accelerometer can be adjusted by changing the fiber length and the end mass that is attached to the fiber end. In addition, FBGs in a twin-core fiber have also been used for an acceleration sensor [51], but since two cores (one core is located in the fiber center) can only determine the curvature in a one-dimensional plane, it can be used as a one-axis accelerometer. While, using several FBGs simultaneously in multiple cores of seven-core fibers, two-dimensional accelerometers have been demonstrated, which are capable of measuring the vibration azimuthal angle as well as the acceleration simultaneously [52,53].

What is more, based on the same principle of the MCF accelerometer, MCF and multifiber inclinometers have also been developed [54,55]. As shown in Figure 18, the inclinometers are made of MCF or multifiber bundle cantilevers, in which FBGs are inscribed in the fiber cores, and a phase generated carrier demodulation technique has been used to extract the differential phases between the FBGs [56,57]. The differential strain measurements of FBGs in three cores (e.g., cores A–C in Figure 18b) can be used to retrieve the bending orientation and bending radius [58], which is then used to calculate the inclination through a transform equation that is derived from the calibration procedure [54]. In addition, fiber Bragg gratings in a seven-core fiber have also been developed in a two-dimensional inclinometer, which is able to measure the azimuthal angle and the inclination angle simultaneously [59].

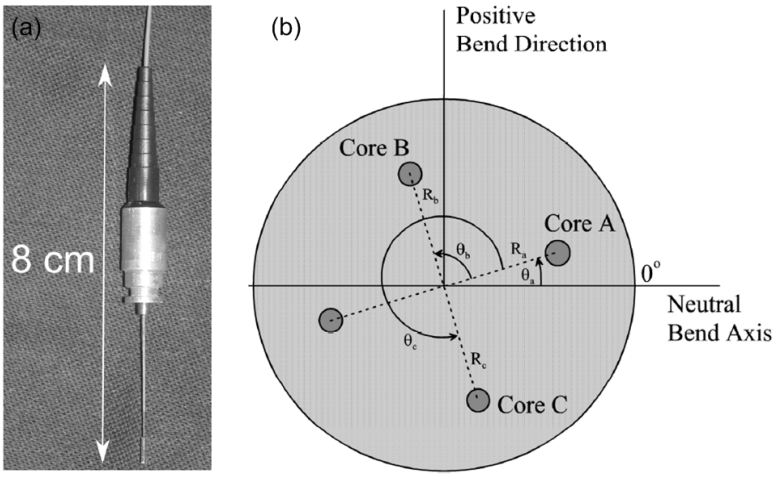

Figure 18. (**a**) The packaged MCF inclinometer. (**b**) Core geometry of the MCF. Bend direction denotes the direction of positive radii of curvature (end of the fiber points down). Neutral bend axis defines the plane of bending. The cores are labeled with their respective core radii and angular offsets from 0°. Figure reproduced from Ref. [54] © 2009 SPIE.

Utilizing the bending sensitivity of off-center cores of the MCF, parametrical fiber three-dimensional (3D) shape sensing has been widely investigated in recent years [60]. The technology relies on the measurement of fiber bending induced strains in multiple cores originally through axially co-located discrete FBGs arrays, then the obtained differential strains are used to retrieve the local bending angles and bending radii along the fiber length, and by using these parameters eventually the overall shape of the MCF can be parametrically reconstructed by solving the Frenet–Serret equations [35,61]. Figure 19 shows an example of MCF enabled shape sensing by using this technology [62]. In order to ensure high shape reconstruction accuracy, the sensing fiber needs to contain high density FBGs arrays, e.g., typically 1 cm spacing [62]. In this case, the interrogation of the Bragg wavelengths of the FBGs is unable to be accomplished by the traditional optical time-domain reflectometry (OTDR) technique due to its bad spatial resolution, i.e., in the order of meters. On the other hand, the wavelength-division multiplexed FBG arrays scheme suffers from finite bandwidth of the light source, which results in very limited multiplexing numbers of FBGs. Therefore, normally the high density FBGs arrays in MCF are measured by using the optical frequency-domain reflectometry (OFDR) technique [62,63], since it can offer up to micrometers spatial resolution.

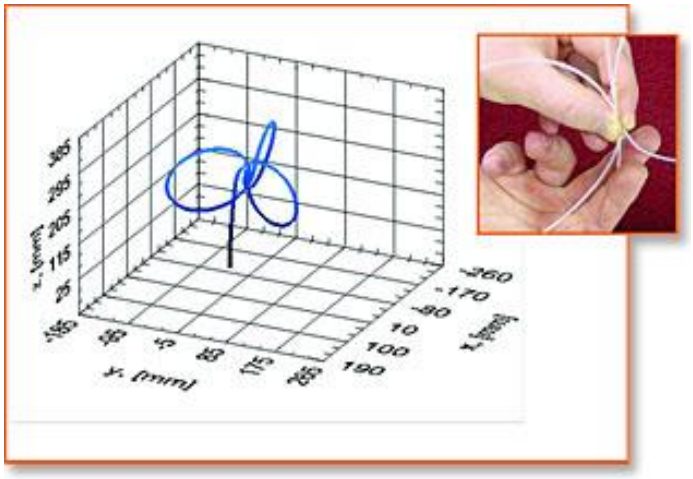

Figure 19. An example of multicore fiber enabled shape measurement. Figure reproduced from Ref. [62] © 2005 SPIE.

It is worth mentioning that when FBG arrays are used to measure the local strains in cores of the MCF, the spatial resolution of strain measurements is determined by the interval of two adjacent FBG groups. As mentioned previously, the interval is typically 1 cm, which might be still insufficient. The sparse discrete sets of strains that are used for shape reconstruction might lead to accumulated large angular error, which rapidly reduces the accuracy of the retrieved shape. Therefore, it turns out that localization of strain with higher spatial resolution is preferred. This can be done by measuring the intrinsic Rayleigh backscattering signals through OFDR, then strain can be retrieved by calculating the cross-correlation of two sets of Rayleigh measurements [64–66]. What is more, in order to increase the signal-to-noise ratio (SNR) of measurement, continuous weak fiber Bragg gratings can be inscribed in the cores of MCF along the whole fiber length [67–69].

As a matter of fact, the sensing fiber may also have an arbitrary twist along the fiber length, so in addition to bending, fiber twist will also give rise to additional strain in the fiber cores, which might cause error in shape reconstruction of the sensing fiber [70,71]. Therefore, fiber twist induced strain needs to be separated from the overall strain measurement in MCF. In order to be able to measure fiber twist, a kind of helical MCF with permanent twisted off-center cores and a straight central core has been developed [72–77]. As an example, Figure 20 presents the schematic diagram of a helical seven core fiber [77], in which continuous weak fiber Bragg gratings have been written in the cores of MCF along

the whole fiber length during the fiber drawing process, so it allows for a fiber twist effect compensated strain measurement with high SNR, which will be very helpful for shape sensing. In fact, in addition to fiber twist, the error of core position as well as inaccurate placement of the FBGs within each cross-section of the MCF will also eventually decrease the accuracy of shape reconstruction [78,79]. Moreover, it is found that the parameters of FBG length, fiber geometry, photo-elastic coefficient, etc., also have an impact on the shape reconstruction accuracy [80,81].

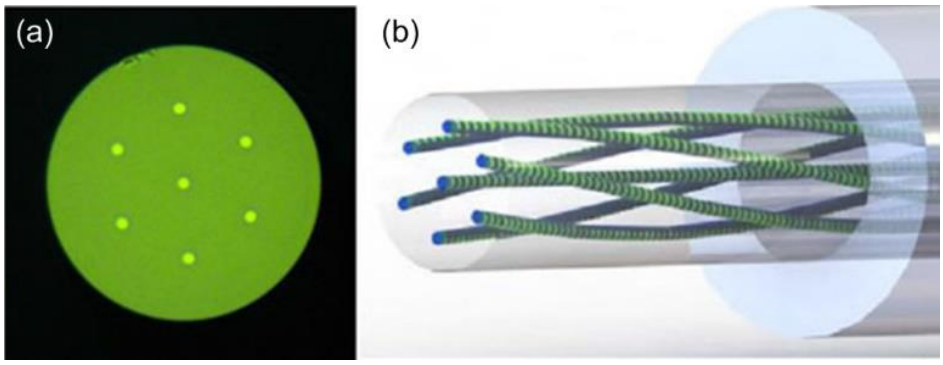

Figure 20. (**a**) End-view image of a seven-core fiber with coating removed; (**b**) twisted multicore fiber schematic showing UV transparent coating (right). Bare glass region (left) shown to highlight twisted multicore continuous gratings. Adapted with permission from Ref. [77] © 2017 IEEE.

In fact, it is realized that precise fully 3D shape sensing using MCF is complicated and difficult, because the angular error will accumulate along the fiber length during shape reconstruction, so the technology is highly dependent on the accuracy of strain measurement and the localization resolution of strain, while MCF enabled curvature sensing turns out to be easier and reliable. So far, multipoint two-dimensional curvature sensing using discrete FBG arrays in MCF [82,83], as well as distributed curvature sensing using the Brillouin optical time domain analysis (BOTDA) technique in MCF have been demonstrated with high accuracy [24]. As for the application fields, MCF enabled curvature and shape sensors have shown great potential in many industrial applications [60], e.g., for real time sensing of a wing's shape in flight, and for medical instruments such as a catheter or robotics that can be integrated into minimally invasive surgery systems [84–87], etc.

Here, it is worth mentioning that writing gratings in MCF turns out to be more complicated than in SMF, due to the geometric difference in spatial position between cores of the MCF, which adds some technical challenges in fabrication, e.g., due to the lens effect of the fiber, the grating strength may have variations between cores, and it may also lead to different transmission/reflection profiles of the FBGs [39,62,76,88–91]. Currently, the most widely used way to write gratings in MCF is to use UV light irradiation, and this method will normally bring in gratings in all cores of the MCF. However, in order to achieve selective FBG inscription in any specific core of a MCF, a femtosecond laser writing method can be used [41,92–94]. In addition, the small spot direct ultraviolet writing technique has also been used to achieve FBG inscription into individual cores of a seven-core fiber [95].

In addition to the widely developed applications for bending and shape sensing, FBGs in MCF have also been used for measuring temperature, strain, and refractive index [96–99], etc. Efforts have also been made for the demodulation of FBG in MCF. For example, a broadband source with a sinusoidal spectrum has been used to interrogate the wavelength of FBGs in MCF [100], which transforms the wavelength shift of FBGs into the variation in reflected power, thus, providing a fast wavelength measurement method. The microwave photonics filtering (MPF) technique has also been used to measure the wavelengths of FBGs in MCF, which retrieves the curvature of fiber by monitoring the notch frequency shift of the MPF, offering a high resolution curvature measurement solution [101]. On the other hand, it is worth mentioning that similar functionality to MCF has been achieved by using a fiber bundle that is composed of multiple single mode fibers, in which FBGs

have been inscribed, and they have been used to measure inclinometer [55], curvature and temperature [102], as well as 2D flow velocity [103], etc.

4. MCF-Based Tilted Fiber Bragg Grating Sensors

In addition to the conventional FBG, tilted fiber Bragg grating (TFBG) has also been written in MCF. As shown in Figure 21, inter-core crosstalk induced by TFBG has been observed in a seven-core fiber [104], including forward transmission crosstalk and backward reflection crosstalk. As an example, Figure 21b shows the measured transmission spectrum, crosstalk, and back crosstalk between core 1 and core 3. The experimental result also indicates that the magnitude and direction of fiber bending, as well as the external refractive index have an impact on the inter-core crosstalk, which might be used for sensing applications. For example, the inter-core crosstalk caused by TFBG in MCF has been used for temperature and surrounding refractive index sensing [105]. The result shows that for refractive index sensing, the higher the tilted angle the higher the sensor sensitivity.

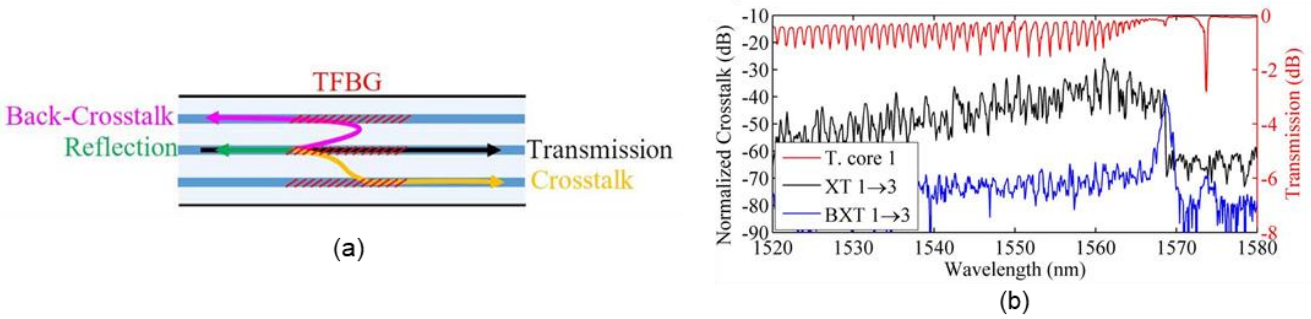

Figure 21. (**a**) Schematic diagram of the MCF with TFBG inscribed, showing inter-core crosstalk induced by TFBG; (**b**) transmission spectra of inscribed TFBG, crosstalk, and back crosstalk between cores 1 and 3. Adapted with permission from Ref. [104] © 2017 Optica Publishing Group.

Tilted fiber Bragg gratings in 4-core fibers have also been used to develop refractometers [106]. Thanks to the reduction in the core-surrounding medium distance in the multicore fiber, higher sensitivity can be achieved in comparison with their counterparts in SMF. Particularly, a plasmonic sensor-based refractometer was demonstrated using gold-coated TFBG in the 4-core fiber, which brought a 10fold sensitivity increase, showing great potential for biosensing applications. However, it is worth mentioning that so far the number of investigations on the MCF-TFBG sensor is still very low, which is much less than that of the MCF based FBG sensors and LPG sensors. It is believed that MCF will enable more TFBG based sensing applications in the future.

5. MCF-Based Long Period Grating Sensors

Long period gratings (LPGs) have also been inscribed in MCFs [107–111]. Similar to the characteristic of FBG in MCF, LPG in MCF is also bending sensitive, owing to the reason that fiber bending will give rise to tangential strain in off-center positions of the fiber. The bending dependence of LPGs in a seven-core fiber has been characterized, as shown in Figure 22 [108]. The seven-core fiber contains six outer cores that are arranged in a hexagonal pattern and a central core. The resonant wavelength shift of each LPG as a function of curvature is presented in Figure 22a, where the fiber is placed at the straight position. The bending angle dependence of the resonant wavelength under a constant curvature of 1.25 m^{-1} has also been measured, as shown in Figure 22b, which shows sinusoidal response curves, owing to the angular dependence of the strain caused by fiber bending. It is also worth mentioning that LPG in MCF is also found to be sensitive to torsion [108].

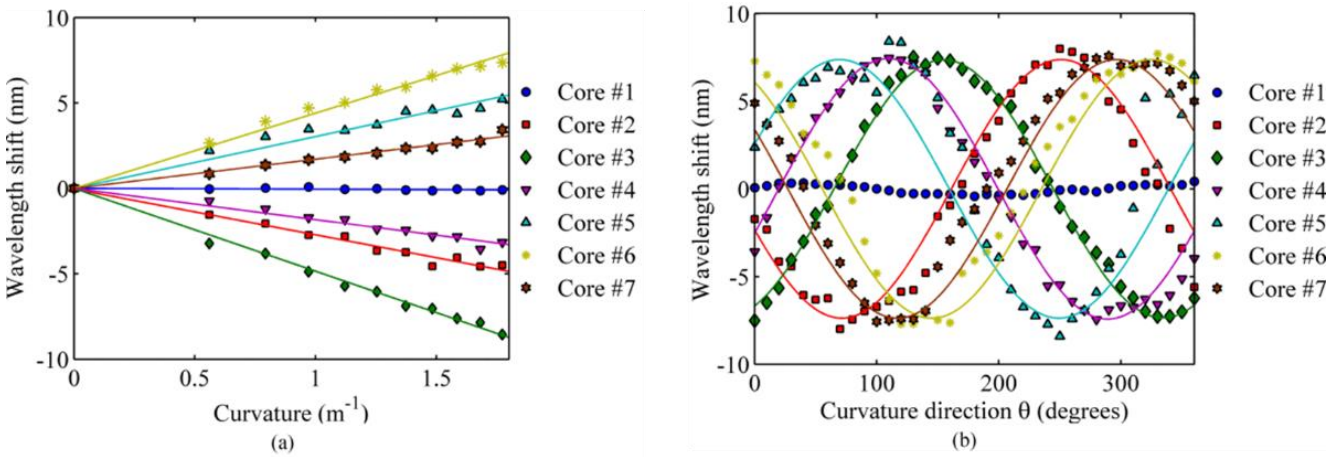

Figure 22. (**a**) Wavelength shift with the curvature magnitude. (**b**) Wavelength shift with curvature direction at a constant curvature of 1.25 m^{-1}. Adapted with permission from Ref. [108] © 2018 IEEE.

LPGs in a three-core fiber have also been used to develop a two-dimensional microbend sensor [109]. As shown in Figure 23, the three-core fiber consists of one central core and two outer cores with isosceles triangle arrangement and 120° angular offset. LPGs with different periods have been written in the two outer cores, therefore, different resonant wavelengths are obtained, as shown in Figure 23. The resonant wavelength shift of the two LPGs as a function of curvature under different bending angles has been measured, as shown in Figure 23c [109]. It is then proposed that the calibrated result can be used to estimate a coordinate system whose x- and y-axis are the resonant wavelengths of the two LPGs, respectively, as shown in Figure 23d. Therefore, the coordinate can be used to infer the bending angle. Quantitatively, this is achieved by calculating a matrix. As has been mentioned previously, since the curvature sensitivity s_i (obtained from Figure 23c) of LPG in the MCF follows a sinusoidal response curve, which can be fitted by

$$s_i = y_i + A_i \sin(\theta - \theta_i),\ i = 1,\ 2 \tag{11}$$

where θ is the bending angle, and the other parameters can be determined by experiments. Then, curvature C and bending angle θ can be obtained by calculating the matrix

$$\begin{bmatrix} \Delta\lambda_1 \\ \Delta\lambda_2 \end{bmatrix} = C \cdot \begin{bmatrix} y_1 + A_1 \sin(\theta - \theta_1) \\ y_2 + A_2 \sin(\theta - \theta_2) \end{bmatrix} \tag{12}$$

where $\Delta\lambda_1$ and $\Delta\lambda_2$ are the resonant wavelength shifts of the two LPGs.

LPGs in a seven-core fiber have also been used for external refractive index sensing, where the surface of MCF is partially coated by a thin film SnO_2 layer [110]. In addition to the widely used UV irradiation method, LPGs have also been generated in a heterogeneous seven-core fiber through electrical arc discharges by using a commercial fiber fusion splicer [111]. The LPGs in heterogeneous cores have been used for strain and temperature discriminative sensing.

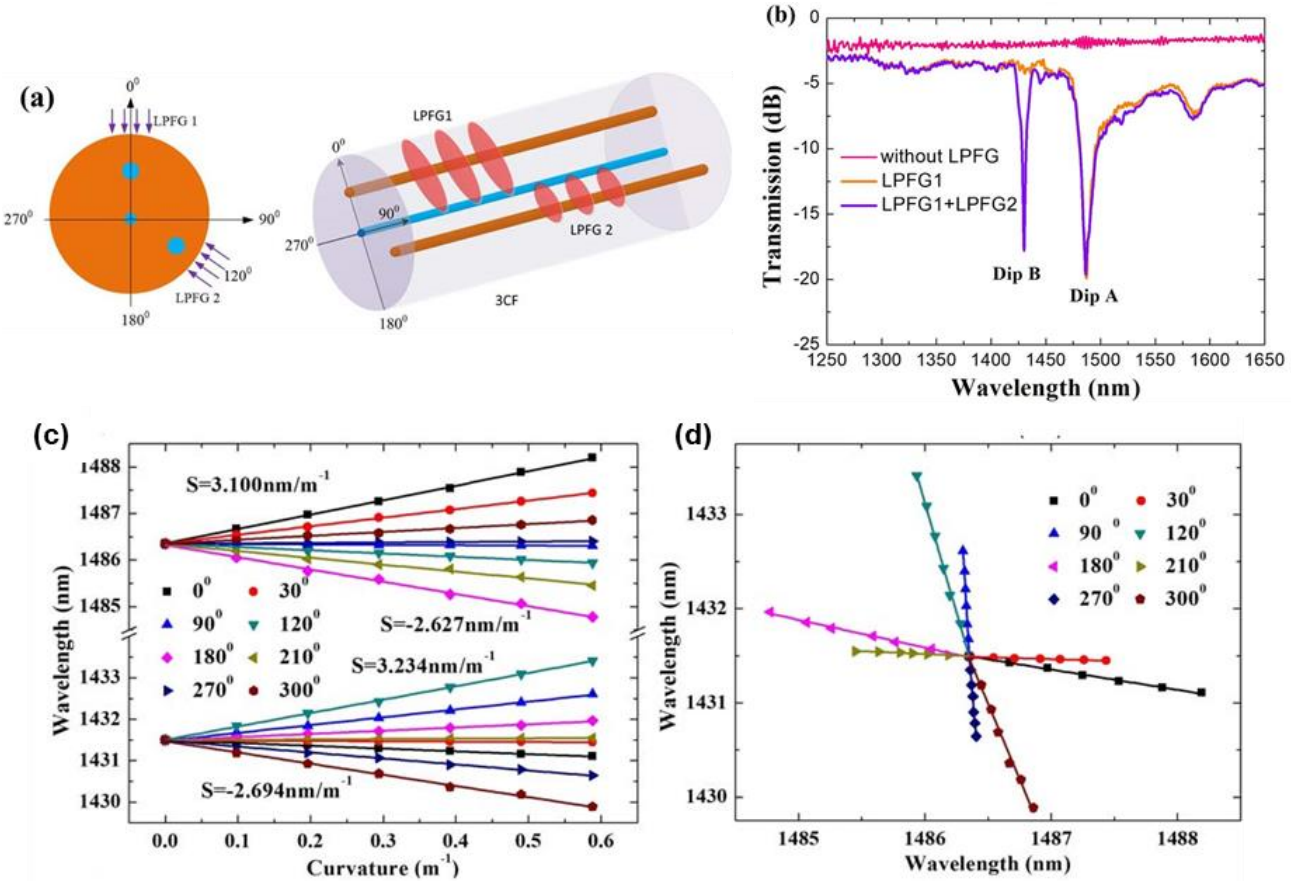

Figure 23. (**a**) Schematic diagram of the LPFGs in the three-core fiber; (**b**) measured transmission spectra of the LPFG1 and LPFG2; (**c**) measured resonance wavelength as a function of curvature for different orientations; (**d**) bending vector sensing coordinate system. Adapted with permission from Ref. [109] © 2017 Optica Publishing Group.

6. Discussion

Thanks to the unique structure of multicore fiber, which contains multiple cores in a single fiber cladding, multicore fiber turns out to be an excellent platform with unprecedented advantages that allows to develop diverse functional lab-on-fiber devices, with much better flexibility and diversity than the normal single mode fiber. So far, multicore fibers have been used to fabricate various in-fiber integrated devices and sensors, e.g., a variety of MCF gratings and interferometers. Particularly, owing to the bending sensitivity in off-center cores, multicore fibers have opened up a new field of sensing applications, i.e., bending and 3D shape sensing. A summary of various multicore fiber sensors is presented, as shown in Table 1.

Despite the exciting developments and bright future of multicore fiber sensors, there are still some critical issues that need to be addressed. Firstly, it remains a technical challenge to manipulate an individual core in the multicore fiber due to the restriction imposed by the geometric structure and lens effect of the fiber, e.g., it is difficult to write fiber gratings or fabricate interferometers with different properties in distinct cores in co-located positions of a multicore fiber. In order to enable lab-on-fiber application, high-precision core-selective fabrication technology is required in the future. Secondly, though MCF has been widely developed for bending and shape sensing, it requires calibration of the original azimuthal angle that is used for reference. Unfortunately, high precision position calibration is difficult due to the small size of the fiber. The angular deflection of the original fiber placement turns out to be one of the major factors that cause error in bending sensing. In addition, another problem is the low bending sensitivity of fiber

gratings, as a result it is difficult to retrieve small curvature change, especially when the bending radius is large, which also leads to large error in shape reconstruction. Therefore, it is necessary to improve the sensitivity of bending measurement. This may be done by using a MCF that has a larger distance from the off-center core to the fiber center, as inferred from Equation (1), i.e., the longer the distance, the higher the bending sensitivity. In addition, instead of using fiber gratings, other high sensitivity sensing techniques can also be employed in bending and shape measurement, e.g., phase-sensitive optical time-domain reflectometry (φ-OTDR) [112], etc. However, it should be pointed out that the meter-scale spatial resolution of φ-OTDR is not comparable with that of FBG. Finally, it is worth mentioning that, comparing with the traditional widely used curvature sensing scheme employing optical fiber modal interferometers [113], MCF grating-based curvature sensors have the merits of being compact, robust, and having excellent mechanical strength, but their curvature sensitivity may not be comparable with some of the modal interferometer-based curvature sensors.

Table 1. Summary of different multicore fiber sensors.

Type of Sensor	Application	Principle/Feature	Refs.
MCF-based FBG sensor	Bending/curvature sensing	Fiber bending causes differential response in different cores	[37–39,41–43,82,83,100,101]
	Transverse loading sensing	Transverse stress causes birefringence change	[44,45]
	Vibration sensing	Fiber bending causes output power change of FBGs	[47]
	Displacement sensing	Displacement causes fiber curvature change	[48]
	Acceleration sensing	Fiber bending causes differential strain in different cores	[49–53]
	Inclinometer sensor	Fiber bending causes differential strain in different cores	[54,55,59]
	3-D shape sensing	Differential strain in different cores	[35,60–62,64,68,71,73,74,77–81,84–87]
	Temperature, strain sensing	Temperature and strain sensitivity	[96,97]
	Refractive index sensing	Using etched multicore fiber	[98,99]
MCF-based TFBG sensor	Temperature, curvature and refractive index sensing	Inter-core crosstalk, surface plasmon resonance	[104–106]
MCF-based LPG sensor	Bending sensing	Fiber bending causes wavelength shift of LPGs	[107–109]
	Refractive index sensing	Fiber surface is partially coated with a thin film SnO_2 layer	[110]
MCF-based distributed fiber sensor	Temperature, strain sensing	Temperature and strain sensitivity	[111]
	Curvature and 3-D shape sensing	Measuring the differential strain using BOTDA technique	[24]
	Temperature and strain discriminative sensing	Hybrid Raman and Brillouin sensor, or using heterogeneous multicore fiber	[25,26]
	High performance distributed fiber sensing	Large dynamic range and ultra-high measurement resolution simultaneously	[27]
	Multi-parameter sensing	Using a hybrid sensing system, e.g., DTS and DAS, simultaneously	[28,29]
	Distributed vibration sensing	MCF interferometer enables wide frequency measurement range	[30,31]

7. Conclusions

In this review, a comprehensive survey of research progress on multicore fiber grating sensors was presented. Several key aspects of the achievements using the multicore fiber in fiber grating sensing systems are summarized, including multicore fiber-based fiber Bragg grating sensors, tilted fiber Bragg grating sensors, and long period grating sensors. In addition to the traditional sensing applications, e.g., measuring temperature, stain, and refractive index, etc., the unique bending sensitivity in off-center cores of MCF has been widely developed for bending/curvature sensing or measuring physical parameters that are associated with bending, e.g., transverse loading, acceleration, vibration, flow velocity of liquid and gas, and 3D shape, etc. Thanks to the structure of multiple parallel cores in MCF, it shows unprecedented advantages in allowing to develop diverse functional lab-on-

fiber devices, and it is believed that multicore fibers will enable more exciting applications in the future.

Author Contributions: Conceptualization, Z.Z.; writing—original draft preparation, Z.Z. and Y.D.; writing—review and editing, Z.Z. and M.T. All authors have read and agreed to the published version of the manuscript.

Funding: This research was funded by the National Key Research and Development Program of China (2021YFB2800902), National Natural Science Foundation of China (61931010, 62105111), Hubei Province Key Research and Development Program (2021BAA008), Fundamental Research Funds for the Central Universities (HUST: 2021XXJS026), and Natural Science Foundation of Hubei Province (2021CFB049).

Data Availability Statement: Not applicable.

Conflicts of Interest: The authors declare no conflict of interest.

References

1. Winzer, P.J. Making spatial multiplexing a reality. *Nat. Photonics* **2014**, *8*, 345–348. [CrossRef]
2. Van Uden, R.G.H.; Correa, R.A.; Lopez, E.A.; Huijskens, F.M.; Xia, C.; Li, G.; Schülzgen, A.; Waardt, H.; Koonen, A.M.J.; Okonkwo, C.M. Ultra-high-density spatial division multiplexing with a few-mode multicore fibre. *Nat. Photonics* **2014**, *8*, 865–870. [CrossRef]
3. Tang, M. Multicore Fibers. In *Handbook of Optical Fibers*; Peng, G.D., Ed.; Springer: Singapore, 2019. [CrossRef]
4. Ortiz, A.M.; Sáez, R.L. Multi-core optical fibers: Theory, applications and opportunities. In *Selected Topics on Optical Fiber Technologies and Applications*; IntechOpen: London, UK, 2017; pp. 63–102.
5. Awaji, Y.; Saitoh, K.; Matsuo, S. *Optical Fiber Telecommunications VIB: Chapter 13. Transmission Systems Using Multicore Fibers*; Elsevier: Amsterdam, The Netherlands, 2013.
6. Glas, P.; Naumann, M.; Schirrmacher, A.; Pertsch, T. The multicore fiber–a novel design for a diode pumped fiber laser. *Opt. Commun.* **1998**, *151*, 187–195. [CrossRef]
7. Mizuno, T.; Takara, H.; Sano, A.; Miyamoto, Y. Dense space-division multiplexed transmission systems using multi-core and multi-mode fiber. *J. Lightwave Technol.* **2015**, *34*, 582–592. [CrossRef]
8. Zhu, B.; Taunay, T.F.; Yan, M.F.; Fini, J.M.; Fishteyn, M.; Monberg, E.M.; Dimarcello, F.V. Seven-core multicore fiber transmissions for passive optical network. *Opt. Express* **2010**, *18*, 11117–11122. [CrossRef] [PubMed]
9. Matsui, T.; Sakamoto, T.; Goto, Y.; Saito, K.; Nakajima, K.; Yamamoto, F.; Kurashima, T. Design of 125 μm cladding multi-core fiber with full-band compatibility to conventional single-mode fiber. In Proceedings of the 2015 European Conference on Optical Communication (ECOC), Valencia, Spain, 27 September–1 October 2015; pp. 1–3.
10. Takara, H.; Sano, A.; Kobayashi, T.; Kubota, H.; Kawakami, H.; Matsuura, A.; Miyamoto, Y.; Abe, Y.; Ono, H.; Shikama, K.; et al. 1.01-Pb/s (12 SDM/222 WDM/456 Gb/s) crosstalk-managed transmission with 91.4-b/s/Hz aggregate spectral efficiency. In Proceedings of the European Conference and Exhibition on Optical Communication, Amsterdam, The Netherlands, 16–20 September 2012; p. Th-3.
11. Li, M.J.; Hoover, B.; Nazarov, V.N.; Butler, D.L. Multicore fiber for optical interconnect applications. In Proceedings of the 2012 17th Opto-Electronics and Communications Conference, Busan, Korea, 2–6 July 2012; pp. 564–565.
12. Saitoh, K.; Matsuo, S. Multicore fiber technology. *J. Lightwave Technol.* **2016**, *34*, 55–66. [CrossRef]
13. Takenaga, K.; Arakawa, Y.; Tanigawa, S.; Guan, N.; Matsuo, S.; Saitoh, K.; Koshiba, M. Reduction of crosstalk by trench-assisted multi-core fiber. In Proceedings of the Optical Fiber Communication Conference 2011, Los Angeles, CA, USA, 6–10 March 2011; Optical Society of America: Washington, DC, USA, 2011; p. OWJ4.
14. Xia, C.; Bai, N.; Ozdur, I.; Zhou, X.; Li, G. Supermodes for optical transmission. *Opt. Express* **2011**, *19*, 16653–16664. [CrossRef]
15. Klaus, W.; Sakaguchi, J.; Puttnam, B.J.; Awaji, Y.; Wada, N.; Kobayashi, T.; Watanabe, M. Free-space coupling optics for multicore fibers. *IEEE Photonics Technol. Lett.* **2012**, *24*, 1902–1905. [CrossRef]
16. Tottori, Y.; Kobayashi, T.; Watanabe, M. Low loss optical connection module for seven-core multicore fiber and seven single-mode fibers. *IEEE Photonics Technol. Lett.* **2012**, *24*, 1926–1928. [CrossRef]
17. Thomson, R.R.; Bookey, H.T.; Psaila, N.D.; Fender, A.; Campbell, S.; Macpherson, W.N.; Barton, J.S.; Reid, D.T.; Kar, A.K. Ultrafast-laser inscription of a three dimensional fan-out device for multicore fiber coupling applications. *Opt. Express* **2007**, *15*, 11691–11697. [CrossRef]
18. Watanabe, K.; Saito, T.; Imamura, K.; Shiino, M. Development of fiber bundle type fan-out for multicore fiber. In Proceedings of the 2012 17th Opto-Electronics and Communications Conference, Busan, Korea, 2–6 July 2012; pp. 475–476.
19. Noordegraaf, D.; Skovgaard, P.M.W.; Nielsen, M.D.; Bland-Hawthorn, J. Efficient multi-mode to single-mode coupling in a photonic lantern. *Opt. Express* **2009**, *17*, 1988–1994. [CrossRef] [PubMed]
20. Li, B.; Feng, Z.; Tang, M.; Xu, Z.; Fu, S.; Wu, Q.; Deng, L.; Tong, W.; Liu, S.; Shum, P.P. Experimental demonstration of large capacity WSDM optical access network with multicore fibers and advanced modulation formats. *Opt. Express* **2015**, *23*, 10997–11006. [CrossRef] [PubMed]

21. Tang, M.; Zhao, Z.; Gan, L.; Wu, H.; Wang, R.; Li, B.; Fu, S.; Liu, S.; Liu, D.; Wei, H.; et al. Spatial-division multiplexed optical sensing using MCF and FMF. In Proceedings of the Specialty Optical Fibers 2016, Vancouver, BC, Canada, 18–20 July 2016; Optical Society of America: Washington, DC, USA, 2016; p. SoM2G.3.
22. Zhao, Z.; Tang, M.; Lu, C. Distributed multicore fiber sensors. *Opto-Electron. Adv.* **2020**, *3*, 02190024. [CrossRef]
23. Zhao, Z.; Tang, M. Distributed fiber sensing using SDM fibers. In Proceedings of the Optoelectronics and Communications Conference 2021, Hong Kong, China, 3–7 July 2021; Optical Society of America: Washington, DC, USA, 2021; p. W4D.1.
24. Zhao, Z.; Soto, M.A.; Tang, M.; Thévenaz, L. Distributed shape sensing using Brillouin scattering in multi-core fibers. *Opt. Express* **2016**, *24*, 25211–25223. [CrossRef] [PubMed]
25. Zhao, Z.; Dang, Y.; Tang, M.; Duan, L.; Wang, M.; Wu, H.; Fu, S.; Tong, W.; Shum, P.P.; Liu, D. Spatial-division multiplexed hybrid Raman and Brillouin optical time-domain reflectometry based on multi-core fiber. *Opt. Express* **2016**, *24*, 25111–25118. [CrossRef]
26. Zhao, Z.; Dang, Y.; Tang, M.; Li, B.; Gan, L.; Fu, S.; Wei, H.; Tong, W.; Shum, P.; Liu, D. Spatial-division multiplexed Brillouin distributed sensing based on a heterogeneous multicore fiber. *Opt. Lett.* **2017**, *42*, 171–174. [CrossRef]
27. Dang, Y.; Zhao, Z.; Tang, M.; Zhao, C.; Gan, L.; Fu, S.; Liu, T.; Tong, W.; Shum, P.P.; Liu, D. Towards large dynamic range and ultrahigh measurement resolution in distributed fiber sensing based on multicore fiber. *Opt. Express* **2017**, *25*, 20183–20193. [CrossRef]
28. Zhao, Z.; Dang, Y.; Tang, M.; Wang, L.; Gan, L.; Fu, S.; Yang, C.; Tong, W.; Lu, C. Enabling simultaneous DAS and DTS through space-division multiplexing based on multicore fiber. *J. Lightwave Technol.* **2018**, *36*, 5707–5713. [CrossRef]
29. Dang, Y.; Zhao, Z.; Wang, X.; Liao, R.; Lu, C. Simultaneous distributed vibration and temperature sensing using multicore fiber. *IEEE Access* **2019**, *7*, 151818–151826. [CrossRef]
30. Zhao, Z.; Shen, L.; Dang, Y.; Lu, C.; Tang, M. Enabling long range distributed vibration sensing using multicore fiber interferometers. *Opt. Lett.* **2021**, *46*, 3685–3688. [CrossRef]
31. Zhao, Z.; Tang, M.; Wang, L.; Guo, N.; Tam, H.Y.; Lu, C. Distributed vibration sensor based on space-division multiplexed reflectometer and interferometer in multicore fiber. *J. Lightwave Technol.* **2018**, *36*, 5764–5772. [CrossRef]
32. Zhao, Z.; Tang, M.; Fu, S.; Liu, S.; Wei, H.; Cheng, Y.; Tong, W.; Shum, P.; Liu, D. All-solid multi-core fiber-based multipath Mach–Zehnder interferometer for temperature sensing. *Appl. Phys. B* **2013**, *112*, 491–497. [CrossRef]
33. Zhao, Z.; Liu, Z.; Tang, M.; Fu, S.; Wang, L.; Guo, N.; Jin, C.; Tam, H.Y.; Lu, C. Robust in-fiber spatial interferometer using multicore fiber for vibration detection. *Opt. Express* **2018**, *26*, 29629–29637. [CrossRef] [PubMed]
34. Duan, L.; Zhang, P.; Tang, M.; Wang, R.; Zhao, Z.; Fu, S.; Gan, L.; Zhu, B.; Tong, W.; Liu, D.; et al. Heterogeneous all-solid multicore fiber based multipath Michelson interferometer for high temperature sensing. *Opt. Express* **2016**, *24*, 20210–20218. [CrossRef]
35. Moore, J.P.; Rogge, M.D. Shape sensing using multi-core fiber optic cable and parametric curve solutions. *Opt. Express* **2012**, *20*, 2967–2973. [CrossRef]
36. Zhao, Z.; Soto, M.A.; Tang, M.; Thévenaz, L. Curvature and shape distributed sensing using Brillouin scattering in multicore fibers. In Proceedings of the Optical Sensors 2016, Vancouver, BC, Canada, 18–20 July 2016; Optical Society of America: Washington, DC, USA, 2016; p. SeM4D.4.
37. Gander, M.J.; MacPherson, W.N.; McBride, R.; Jones, J.D.; Zhang, L.; Bennion, I.; Blanchard, P.M.; JBurnett, J.G.; Greenaway, A.H. Bend measurement using Bragg gratings in multicore fibre. *Electron. Lett.* **2000**, *36*, 120–121. [CrossRef]
38. Flockhart, G.M.H.; MacPherson, W.N.; Barton, J.S.; Jones, J.D.C.; Zhang, L.; Bennion, I. Two-axis bend measurement with Bragg gratings in multicore optical fiber. *Opt. Lett.* **2003**, *28*, 387–389. [CrossRef]
39. Zhang, H.; Wu, Z.; Shum, P.P.; Wang, R.; Dinh, X.Q.; Fu, S.; Tong, W.; Tang, M. Fiber Bragg gratings in heterogeneous multicore fiber for directional bending sensing. *J. Opt.* **2016**, *18*, 085705. [CrossRef]
40. Zhou, W.; Zhou, Y.; Dong, X.; Shao, L.; Cheng, J.; Albert, J. Fiber-optic curvature sensor based on cladding-mode Bragg grating excited by fiber multimode interferometer. *IEEE Photonics J.* **2012**, *4*, 1051–1057. [CrossRef]
41. Yang, K.; He, J.; Liao, C.; Wang, Y.; Liu, S.; Guo, K.; Zhou, J.; Li, Z.; Tan, Z.; Wang, Y. Femtosecond laser inscription of fiber Bragg grating in twin-core few-mode fiber for directional bend sensing. *J. Lightwave Technol.* **2017**, *35*, 4670–4676. [CrossRef]
42. Hou, M.; Yang, K.; He, J.; Xu, X.; Ju, S.; Guo, K.; Wang, Y. Two-dimensional vector bending sensor based on seven-core fiber Bragg gratings. *Opt. Express* **2018**, *26*, 23770–23781. [CrossRef] [PubMed]
43. Chen, X.; Zhang, C.; Webb, D.J.; Kalli, K.; Peng, G.D. Highly sensitive bend sensor based on Bragg grating in eccentric core polymer fiber. *IEEE Photonics Technol. Lett.* **2010**, *22*, 850–852. [CrossRef]
44. Silva-Lopez, M.; Li, C.; MacPherson, W.N.; Moore, A.J.; Barton, J.S.; Jones, J.D.; Zhao, D.; Zhang, L.; Bennion, I. Differential birefringence in Bragg gratings in multicore fiber under transverse stress. *Opt. Lett.* **2004**, *29*, 2225–2227. [CrossRef]
45. Silva-Lopez, M.; MacPherson, W.N.; Li, C.; Moore, A.J.; Barton, J.S.; Jones, J.D.; Zhao, D.; Zhang, L.; Bennion, I. Transverse load and orientation measurement with multicore fiber Bragg gratings. *Appl. Opt.* **2005**, *44*, 6890–6897. [CrossRef] [PubMed]
46. MacPherson, W.N.; Flockhart, G.M.; Maier, R.R.; Barton, J.S.; Jones, J.D.; Zhao, D.; Zhang, L.; Bennion, I. Pitch and roll sensing using fibre Bragg gratings in multicore fibre. *Meas. Sci. Technol.* **2014**, *15*, 1642–1646. [CrossRef]
47. Fender, A.; Rigg, E.J.; Maier, R.R.; MacPherson, W.N.; Barton, J.S.; Moore, A.J.; Jones, J.D.; Zhao, D.; Zhang, L.; Bennion, I.; et al. Dynamic two-axis curvature measurement using multicore fiber Bragg gratings interrogated by arrayed waveguide gratings. *Appl. Opt.* **2006**, *45*, 9041–9048. [CrossRef]

48. MacPherson, W.N.; Silva-Lopez, M.; Barton, J.S.; Moore, A.J.; Jones, J.D.C.; Zhao, D.; Zhang, L.; Bennion, I.; Metje, N.; Rogers, C.D.F.; et al. Tunnel monitoring using multicore fiber displacement sensor. *Meas. Sci. Technol.* **2006**, *17*, 1180–1185. [CrossRef]
49. Fender, A.; MacPherson, W.N.; Maier, R.; Barton, J.S.; George, D.S.; Howden, R.I.; Smith, G.W.; Jones, B.J.; McCulloch, S.; Chen, X.; et al. Two-axis temperature-insensitive accelerometer based on multicore fiber Bragg gratings. *IEEE Sens. J.* **2008**, *8*, 1292–1298. [CrossRef]
50. Fender, A.; MacPherson, W.N.; Maier, R.R.J.; Barton, J.S.; George, D.S.; Howden, R.I.; Smith, G.W.; Jones, B.J.; McCulloch, S.; Chen, X.; et al. Two-axis accelerometer based on multicore fibre Bragg gratings. In Proceedings of the Third European Workshop on Optical Fibre Sensors, Napoli, Italy, 4–6 July 2007; International Society for Optics and Photonics: Bellingham, WA, USA, 2007; Volume 6619, p. 66190Q.
51. He, X.; Dong, X. Accelerometer Based on the FBG Inscribed in a Twin-Core Fiber. In Proceedings of the Asia Communications and Photonics Conference 2013, Beijing China, 12–15 November 2013; Optical Society of America: Washington, DC, USA, 2013; p. AF2I.16.
52. Cui, J.; Liu, Z.; Gunawardena, D.S.; Zhao, Z.; Tam, H.Y. Two-dimensional vector accelerometer based on Bragg gratings inscribed in a multi-core fiber. *Opt. Express* **2019**, *27*, 20848–20856. [CrossRef]
53. Zhou, R.; Chen, F.; Li, S.; Wang, R.; Qiao, X. Three-Dimensional Vector Accelerometer Using a Multicore Fiber Inscribed with Three FBGs. *J. Lightwave Technol.* **2021**, *39*, 3244–3250. [CrossRef]
54. Miller, G.A.; Askins, C.G.; Cranch, G.A. Interferometric interrogation of a multicore fiber, two-axis inclinometer. In Proceedings of the 20th International Conference on Optical Fibre Sensors, Edinburgh, UK, 5–9 October 2009; International Society for Optics and Photonics: Bellingham, WA, USA, 2009; Volume 7503, p. 75032R.
55. Miller, G.A. Fabrication of a multifiber optical inclinometer. *IEEE Photon. Technol. Lett.* **2015**, *27*, 1289–1292. [CrossRef]
56. Flockhart, G.M.H.; Cranch, G.A.; Kirkendall, C.K. Differential phase tracking applied to Bragg gratings in multicore fiber for high-accuracy curvature measurement. In Proceedings of the Smart Structures and Materials 2006: Smart Sensor Monitoring Systems and Applications, San Diego, CA, USA, 27 February–1 March 2006; International Society for Optics and Photonics: Bellingham, WA, USA, 2006; Volume 6167, p. 616701.
57. Flockhart, G.M.H.; Cranch, G.A.; Kirkendall, C.K. Differential phase tracking applied to Bragg gratings in multi-core fibre for high accuracy curvature measurement. *Electron. Lett.* **2006**, *42*, 390–391. [CrossRef]
58. Askins, C.G.; Miller, G.A.; Friebele, E.J. Bend and twist sensing in a multiple-core optical fiber. In Proceedings of the 2008 Conference on Optical Fiber Communication/National Fiber Optic Engineers Conference, San Diego, CA, USA, 24–28 February 2008; pp. 1–3.
59. Cui, J.; Gunawardena, D.S.; Liu, Z.; Zhao, Z.; Tam, H.Y. All-fiber two-dimensional inclinometer based on Bragg gratings inscribed in a seven-core multi-core fiber. *J. Lightwave Technol.* **2020**, *38*, 2516–2522. [CrossRef]
60. Amanzadeh, M.; Aminossadati, S.M.; Kizil, M.S.; Rakic, A.D. Recent developments in fibre optic shape sensing. *Measurement* **2018**, *128*, 119–137. [CrossRef]
61. Moore, J.P. Shape sensing using multi-core fiber. In Proceedings of the 2015 Optical Fiber Communications Conference and Exhibition (OFC), Los Angeles, CA, USA, 22–26 March 2015; pp. 1–3.
62. Duncan, R. *Sensing Shape: Fiber-Bragg-Grating Sensor Arrays Monitor Shape at a High Resolution*; SPIE Newsroom: Bellingham, WA, USA, 2005.
63. Soller, B.J.; Gifford, D.K.; Wolfe, M.S.; Froggatt, M.E. High resolution optical frequency domain reflectometry for characterization of components and assemblies. *Opt. Express* **2005**, *13*, 666–674. [CrossRef]
64. Duncan, R.G.; Froggatt, M.E.; Kreger, S.T.; Seeley, R.J.; Gifford, D.K.; Sang, A.K.; Wolfe, M.S. High-accuracy fiber-optic shape sensing. In Proceedings of the Sensor Systems and Networks: Phenomena, Technology, and Applications for NDE and Health Monitoring 2007, San Diego, CA, USA, 19–21 March 2007; International Society for Optics and Photonics: Bellingham, WA, USA, 2007; Volume 6530, p. 65301S.
65. Froggatt, M.; Moore, J. High spatial resolution distributed strain measurement in optical fiber using Rayleigh scatter. *Appl. Opt.* **1998**, *37*, 1735–1740. [CrossRef]
66. Kreger, S.T.; Gifford, D.K.; Froggatt, M.E.; Soller, B.J.; Wolfe, M.S. High resolution distributed strain or temperature measurements in single-and multi-mode fiber using swept-wavelength interferometry. In Proceedings of the Optical Fiber Sensors 2006, Cancun, Mexico, 23–27 October 2006; Optical Society of America: Washington, DC, USA, 2006; p. ThE42.
67. Guo, H.; Tang, J.; Li, X.; Zheng, Y.; Yu, H.; Yu, H. On-line writing identical and weak fiber Bragg grating arrays. *Chin. Opt. Lett.* **2013**, *11*, 030602.
68. Westbrook, P.S.; Feder, K.S.; Kremp, T.; Taunay, T.F.; Monberg, E.; Kelliher, J.; Ortiz, R.; Bradley, K.; Abedin, K.S.; Au, D.; et al. Integrated optical fiber shape sensor modules based on twisted multicore fiber grating arrays. In Proceedings of the Optical Fibers and Sensors for Medical Diagnostics and Treatment Applications XIV, San Francisco, CA, USA, 1–2 February 2014; International Society for Optics and Photonics: Bellingham, WA, USA, 2014; Volume 8938, p. 89380H.
69. Westbrook, S.P.; Kremp, T.; Feder, K.S.; Ko, W.; Monberg, E.M.; Wu, H.; Simoff, D.A.; Ortiz, R.M. Improving distributed sensing with continuous gratings in single and multi-core fibers. In Proceedings of the Optical Fiber Communication Conference 2018, San Diego, CA, USA, 11–15 March 2018; Optical Society of America: Washington, DC, USA, 2018; p. W1K.1.
70. Floris, I.; Sales, S.; Calderón, P.A.; Adam, J.M. Measurement uncertainty of multicore optical fiber sensors used to sense curvature and bending direction. *Measurement* **2019**, *132*, 35–46. [CrossRef]

71. Khan, F.; Barrera, D.; Sales, S.; Misra, S. Curvature, twist and pose measurements using fiber Bragg gratings in multi-core fiber: A comparative study between helical and straight core fibers. *Sens. Actuators A Phys.* **2021**, *317*, 112442. [CrossRef]
72. Askins, C.G.; Miller, G.A.; Friebele, E.J. Bend and twist sensing in a multi-core optical fiber. In Proceedings of the LEOS 2008-21st Annual Meeting of the IEEE Lasers and Electro-Optics Society, Newport Beach, CA, USA, 9–13 November 2008; pp. 109–110.
73. Froggatt, M.; Klein, J.; Gifford, D. Shape sensing of multiple core optical fiber. In Proceedings of the Applied Industrial Optics: Spectroscopy, Imaging and Metrology, AIO 2011, Toronto, ON, Canada, 10–14 July 2011; Optical Society of America: Washington, DC, USA, 2011; p. AIMB2.
74. Lally, E.M.; Reaves, M.; Horrell, E.; Klute, S.; Froggatt, M.E. Fiber optic shape sensing for monitoring of flexible structures. In Proceedings of the Sensors and Smart Structures Technologies for Civil, Mechanical, and Aerospace Systems 2012, San Diego, CA, USA, 12–15 March 2012; International Society for Optics and Photonics: Bellingham, WA, USA, 2012; Volume 8345, p. 83452Y.
75. Cooper, L.J.; Webb, A.S.; Gillooly, A.; Hill, M.; Read, T.; Maton, P.; Hankey, J.; Bergonzo, A. Design and performance of multicore fiber optimized towards communications and sensing applications. In Proceedings of the Optical Components and Materials XII, San Francisco, CA, USA, 9–11 February 2015; International Society for Optics and Photonics: Bellingham, WA, USA, 2015; Volume 9359, p. 93590H.
76. Westbrook, P.S.; Feder, K.S.; Kremp, T.; Taunay, T.F.; Monberg, E.; Ortiz, R.; Puc, G. Improved uniformity of sensor gratings in offset core fibers with fiber lensing mitigation. In Proceedings of the Optical Fibers and Sensors for Medical Diagnostics and Treatment Applications XVI, San Francisco, CA, USA, 13–14 February 2016; International Society for Optics and Photonics: Bellingham, WA, USA, 2016; Volume 9702, p. 97020J.
77. Westbrook, P.S.; Kremp, T.; Feder, K.S.; Ko, W.; Monberg, E.M.; Wu, H.; Simoff, D.A.; Taunay, T.T.; Ortiz, R.M. Continuous multicore optical fiber grating arrays for distributed sensing applications. *J. Lightw. Technol.* **2017**, *35*, 1248–1252. [CrossRef]
78. Floris, I.; Calderón, P.A.; Sales, S.; Adam, J.M. Effects of core position uncertainty on optical shape sensor accuracy. *Measurement* **2019**, *139*, 21–33. [CrossRef]
79. Pauer, H.; Ledermann, C.; Tuschmann, W.; Woern, H. Non-linear compensation of production inaccuracies and material drift by adjusting the sensor data fusion algorithms for shape sensing based on FBG-optical fibers. In Proceedings of the 2014 International Conference on Multisensor Fusion and Information Integration for Intelligent Systems (MFI), Beijing, China, 28–29 September 2014; pp. 1–5.
80. Floris, I.; Madrigal, J.; Sales, S.; Adam, J.M.; Calderón, P.A. Experimental study of the influence of FBG length on optical shape sensor performance. *Opt. Lasers Eng.* **2020**, *126*, 105878. [CrossRef]
81. Idrisov, R.; Floris, I.; Rothhardt, M.; Bartelt, H. Characterization and calibration of shape sensors based on multicore optical fibre. *Opt. Fiber Technol.* **2021**, *61*, 102319. [CrossRef]
82. Barrera, D.; Gasulla, I.; Sales, S. Multipoint two-dimensional curvature optical fiber sensor based on a nontwisted homogeneous fourcore. *J. Lightw. Technol.* **2015**, *33*, 2445–2450. [CrossRef]
83. Sonoda, N.; Takagi, R.; Saito, I.; Abe, T.; Zhao, S.; Tanaka, Y. Multipoint bending measurement using multicore fiber Bragg grating and two-photon absorption process in Si-APD. *IEEE Sens. J.* **2021**, *21*, 25736–25742. [CrossRef]
84. Moon, H.; Jeong, J.; Kang, S.; Kim, K.; Song, Y.-W.; Kim, J. Fiber Bragg-grating-based ultrathin shape sensors displaying single-channel sweeping for minimally invasive surgery. *Opt. Lasers Eng.* **2014**, *59*, 50–55. [CrossRef]
85. Khan, F.; Denasi, A.; Barrera, D.; Madrigal, J.; Sales, S.; Misra, S. Multi-core optical fibers with Bragg gratings as shape sensor for flexible medical instruments. *IEEE Sens. J.* **2019**, *19*, 5878–5884. [CrossRef]
86. Khan, F.; Donder, A.; Galvan, S.; Baena, F.R.; Misra, S. Pose measurement of flexible medical instruments using fiber bragg gratings in multi-core fiber. *IEEE Sens. J.* **2020**, *20*, 10955–10962. [CrossRef]
87. Al-Ahmad, O.; Ourak, M.; Van Roosbroeck, J.; Vlekken, J.; Vander Poorten, E. Improved fbg-based shape sensing methods for vascular catheterization treatment. *IEEE Robot. Autom. Lett.* **2020**, *5*, 4687–4694. [CrossRef]
88. Lindleyet, E.; Min, S.S.; Leon-Saval, S.; Cvetojevic, N.; Lawrence, J.; Ellis, S.; Bland-Hawthorn, J. Demonstration of uniform multicore fiber Bragg gratings. *Opt. Express* **2014**, *22*, 31575–31581. [CrossRef]
89. Stępień, K.; Slowikowski, M.; Tenderenda, T.; Murawski, M.; Szymanski, M.; Szostkiewicz, L.; Becker, M.; Rothhardt, M.; Bartelt, H.; Mergo, P.; et al. Fiber Bragg gratings in hole-assisted multicore fiber for space division multiplexing. *Opt. Lett.* **2014**, *39*, 3571–3574. [CrossRef] [PubMed]
90. Ishihara, H.; Uemura, H.; Sasaki, Y.; Omichi, K.; Fujisawa, T.; Saitoh, K. Grating inscription to few-mode multi-core optical fiber. In Proceedings of the Asia-Pacific Optical Sensors Conference 2016, Shanghai, China, 11–14 October 2016; Optical Society of America: Washington, DC, USA, 2016; p. Th4A.13.
91. Idrisov, R.; Becker, M.; Rothhardt, M.; Bierlich, J.; Bartelt, H. Optimisation of fibre Bragg gratings inscription in multicore fibres. In Proceedings of the Optical Fiber Sensors 2018, Lausanne, Switzerland, 24–28 September 2018; Optical Society of America: Washington, DC, USA, 2018; p. WF64.
92. Donko, A.; Beresna, M.; Jung, Y.; Hayes, J.; Richardson, D.J.; Brambilla, G. Point-by-point femtosecond laser micro-processing of independent core-specific fiber Bragg gratings in a multi-core fiber. *Opt. Express* **2018**, *26*, 2039–2044. [CrossRef] [PubMed]
93. Lee, K.K.C.; Mariampillai, A.; Haque, M.; Standish, B.A.; Yang, V.X.; Herman, P.R. Temperature-compensated fiber-optic 3D shape sensor based on femtosecond laser direct-written Bragg grating waveguides. *Opt. Express* **2013**, *21*, 24076–24086. [CrossRef]
94. Wolf, A.; Dostovalov, A.; Bronnikov, K.; Babin, S. Arrays of fiber Bragg gratings selectively inscribed in different cores of 7-core spun optical fiber by IR femtosecond laser pulses. *Opt. Express* **2019**, *27*, 13978–13990. [CrossRef]

95. Jantzen, S.L.; Bannerman, R.H.S.; Jantzen, A.; Mennea, P.L.; Smith, D.H.; Gates, J.C.; Boyd, L.J.; Smith, P.G.R.; Holmes, C. Individual inscription of spectrally multiplexed Bragg gratings in optical multicore fibers using small spot direct UV writing. *Opt. Express* **2020**, *28*, 21300–21309. [CrossRef]
96. Suo, R.; Lousteau, J.; Li, H.; Jiang, X.; Zhou, K.; Zhang, L.; MacPherson, W.N.; Bookey, H.T.; Barton, J.S.; Kar, A.K.; et al. Fiber Bragg gratings inscribed using 800 nm femtosecond laser and a phase mask in single and multi-core mid-IR glass fibers. *Opt. Express* **2009**, *17*, 7540–7548. [CrossRef] [PubMed]
97. Zhang, Y.; Zhang, W.; Zhang, Y.; Wang, S.; Yu, L.; Yan, Y. Simultaneous measurement of curvature and temperature based on LP11 mode Bragg grating in seven-core fiber. *Meas. Sci. Technol.* **2017**, *28*, 055101. [CrossRef]
98. Kilic, S.G.; Zhu, Y.; Sheng, Q.; Inci, M.N.; Han, M. Refractometer with etched chirped fiber Bragg grating Fabry–Perot interferometer in multicore fiber. *IEEE Photon. Technol. Lett.* **2019**, *31*, 575–578. [CrossRef]
99. Hu, W.; Li, C.; Cheng, S.; Mumtaz, F.; Du, C.; Yang, M. Etched multicore fiber Bragg gratings for refractive index sensing with temperature in-line compensation. *OSA Contin.* **2020**, *3*, 1058–1067. [CrossRef]
100. Zheng, D.; Madrigal, J.; Chen, H.; Barrera, D.; Sales, S. Multicore fiber-Bragg-grating-based directional curvature sensor interrogated by a broadband source with a sinusoidal spectrum. *Opt. Lett.* **2017**, *42*, 3710–3713. [CrossRef]
101. Zheng, D.; Madrigal, J.; Barrera, D.; Sales, S.; Capmany, J. Microwave photonic filtering for interrogating FBG-based multicore fiber curvature sensor. *IEEE Photon. Technol. Lett.* **2017**, *29*, 1707–1710. [CrossRef]
102. Araújo, F.M.; Ferreira, L.A.; Santos, J.L. Simultaneous determination of curvature, plane of curvature and temperature by use of a miniaturized sensing head based on fibre Bragg gratings. *Appl. Opt.* **2002**, *41*, 2401–2407. [CrossRef] [PubMed]
103. Wolf, B.J.; Morton, J.A.S.; MacPherson, W.B.N.; van Netten, S.M. Bio-inspired all -optical artificial neuromast for 2D flow sensing. *Bioinspir. Biomim.* **2018**, *13*, 026013. [CrossRef] [PubMed]
104. Barrera, D.; Madrigal, J.; Sales, S. Tilted fiber Bragg gratings in multicore optical fibers for optical sensing. *Opt. Lett.* **2017**, *42*, 1460–1463. [CrossRef] [PubMed]
105. Madrigal, J.; Barrera, D.; Sales, S. Refractive index and temperature sensor based on TFBGs in multicore fiber. In Proceedings of the Optical Fiber Sensors 2018, Lausanne, Switzerland, 24–28 September 2018; Optical Society of America: Washington, DC, USA, 2018; p. ThE11.
106. Ortega-Gomez, A.; Loyez, M.; Lobry, M.; Chah, K.; Zubia, J.; Villatoro, J.; Caucheteur, C. Plasmonic sensors based on tilted Bragg gratings in multicore optical fibers. *Opt. Express* **2021**, *29*, 18469–18480. [CrossRef] [PubMed]
107. Saffari, P.; Allsop, T.; Adebayo, A.; Webb, D.; Haynes, R.; Roth, M.M. Long period grating in multicore optical fiber: An ultra-sensitive vector bending sensor for low curvatures. *Opt. Lett.* **2014**, *39*, 3508–3511. [CrossRef]
108. Barrera, D.; Madrigal, J.; Sales, S. Long period gratings in multicore optical fibers for directional curvature sensor implementation. *J. Lightw. Technol.* **2018**, *36*, 1063–1068. [CrossRef]
109. Wang, S.; Zhang, W.; Chen, L.; Zhang, Y.; Geng, P.; Zhang, Y.; Yan, T.; Yu, L.; Hu, W.; Li, Y. Two-dimensional microbend sensor based on long period fiber gratings in an isosceles triangle arrangement three-core fiber. *Opt. Lett.* **2017**, *42*, 4938–4941. [CrossRef]
110. Barrera, S.; Goicoechea, J.; Madrigal, J.; González-Larequi, M.; Arregui, F.J.; Sales, S. Partially coated long period fiber Bragg gratings in multicore optical fibers. In Proceedings of the Optical Sensors 2018, Zurich, Switzerland, 2–5 July 2018; Optical Society of America: Washington, DC, USA, 2018; p. SeM4E.5.
111. Wang, R.; Tang, M.; Fu, S.; Feng, Z.; Tong, W.; Liu, D. Spatially arrayed long period gratings in multicore fiber by programmable electrical arc discharge. *IEEE Photon. J.* **2017**, *9*, 1–10. [CrossRef]
112. Szostkiewicz, Ł.; Soto, M.A.; Yang, Z.; Dominguez-Lopez, A.; Parola, I.; Markiewicz, K.; Pytel, A.; Kołakowska, A.; Napierała, M.; Nasiłowski, T.; et al. High-resolution distributed shape sensing using phase-sensitive optical time-domain reflectometry and multicore fiber. *Opt. Express* **2019**, *27*, 20763–20773. [CrossRef]
113. Wang, Q.; Liu, Y. Review of optical fiber bending/curvature sensor. *Measurement* **2018**, *130*, 161–176. [CrossRef]